Numerical Simulation and Experimental Study of a Sediment Sampler Sampling Based on VOF Method

Shudong He
Hunan University of Science and Technology
YouDuo Peng (ydpeng1964@163.com)
Hunan University of Science and Technology https://orcid.org/0000-0003-1917-8522
Yongping Jin
Hunan University of Science and Technology
Buyan Wan
Hunan University of Science and Technology

Original Article

Keywords: sampler, sampling volume, coring rate, VOF method

Posted Date: July 8th, 2020

DOI: https://doi.org/10.21203/rs.3.rs-40417/v1

Numerical Simulation and Experimental Study of a Sediment Sampler Sampling Based on VOF Method

Shudong He, Youduo Peng*, Yongping Jin, Buyan Wan

National-Local Joint Engineering Laboratory of Marine Resources Exploration Equipment and Safety Technology, Hunan University of Science and Technology, Xiangtan 411201, China.

Corresponding author：Youduo Peng E-mail：ydpeng1964@163.com

Abstract: This paper takes the full-ocean-depth sampling device of the mechanical hand-held sampler as the research object, simulates the soft viscous sediment as non-Newtonian Herschel Bulkley viscoplastic fluid, uses the finite volume method and applies the computational fluid mechanics software Fluent to establish the sediment sampling model.VOF method is used to track multiphase flow interface. The effects of the sampling speed, diameter of the sampling tube, drainage discharge and sediment dynamic viscosity on coring rate and sampling volume are studied. The results show that the sampling volume is negatively correlated with those influencing factors. However, the coring rate decreases with the increase of sampling speed, drainage area ratio at inlet and outlet, and dynamic viscosity of sediment. The coring rate first increases and then decreases with the increase of the diameter of the sampling tube, and the peak value is related to the sampling speed and tube diameter. Then, based on the analysis of the numerical simulation results, a sampling simulation experimental platform is built and the sampling experiment is carried out. It can be concluded that the simulation results tally with the experimental results, with the maximum error being only -4.6%, which further verifies the correctness of the numerical model.

Key words: *sampler; sampling volume; coring rate; VOF method*

1. Introduction

The deep-sea sediment records the evolution process of the deep-sea ancient environment and has great significance for the research and application in the fields such as the marine sedimentary process and structural evolution, paleoceanography, paleomagnetism, seabed mineral resource exploration and life process. An important foundation for marine scientific research is to obtain the original samples of these deep-sea sediment. Therefore, advanced collection methods and technical equipment are urgently needed. [1-4]

In order to meet the sampling requirements, the tubular sampler has become one of the important sampling equipment for sediment acquisition. However, due to the interaction between the sampling tube and the sediment, the original sequence of the sediment is often disrupted; the sediment is often bent and deformed and its length is changed [5].Emery and Dietz et al [6] found that the sediment entering the tube was about 50% of the insertion depth by measuring the sampling rate of the open gravity sampler. Lebel et al [7] also reached a similar conclusion where they thought that sample shortening varied from place to place, but the same individual sample was basically linearly shortened. However, Parker and Sills[8] and Parker[9] have questioned this conclusion. They believed that the sample shortening may be caused by obstacles in entry or by defects due to piston suction. They also believed that the round tubular sampler was easier to produce sample defects than the square sampler. Although McCoy et al. [10] did not study the piston core inlet in detail, but they conducted a photographic analysis of the piston core sampling process, which showed that the sample experienced great deformation when entering the sample tube. Ross and Riedel et al. [11] compared the samples taken by the piston sampler and the gravity sampler, which showed that sometimes the sample taken by the piston sampler was shorter than that taken by the gravity sampler, and sometimes the former was longer than the latter. In these comparisons, the shortening of the sample taken by the gravity sampler was due to the thinning of the sediment, while the shortening of the sample taken by the piston sampler was due to the destruction of the top sample. Hongve. D et al. [12] conducted sampling experiments in lakes with the gravity coring device and the piston coring device, and found that the core was compressed to about 50% of the coring length of the piston coring device. At the same time, the degree of sample shortening depended on both the diameter of the coring device and the sampling speed. For above-mentioned samplers, due to the high sampling speed and blocked drainage, water waves were generated at the front end of the sampling tube, which can wash out surface sediment before the sampling tube entered the water interface [13-14]. In the process of lowering, it is imperative to ensure that the water flow is not obstructed [15-16]. In order to solve the above problems, a vibration sampler with low entry speed appeared. During the sampling process, a thin layer of saturated water sediment was formed on the coring tube, which can reduce the damage to the sediment. Even so, when ooze and clay were taken, the average compaction degree exceeded 40%[17-18]. Thus, it can be seen that any kind of sampling technology would inevitably affect the in-situ structure and size of sediment, and the shortening and discontinuity of samples were related to the structure and sampling speed of the sampler, but the quantitative and qualitative relationship

between them needed further studies.

The sampling process for deep-sea sediment is similar to that of pipe piles driving into undrained saturated soft clay. Therefore, the low disturbance sampling mechanism of deep-sea sediment sampler can be analyzed by means of pipe pile theory. The penetration theory of piles in soft clay can be divided into two types: pure shear theory and hole expansion theory. Pure shear theory regards the penetration of the pile tip as the shear failure process of local soil mass which is regarded as rigid-plastic non-volume change material, and uses limit equilibrium theory to solve the ultimate resistance of the penetration of the pile tip. Pure shear mechanism cannot reflect the deformation phenomenon of soil plastic zone [19-21]. Hole expansion theory regards pile sinking as hole expansion in infinite soil. Based on Mohr Coulomb shear strength, stress and deformation distribution are studied by using elastoplastic theory. Carret et al. [22] regarded the sampling process as the expansion of cylindrical hole in soil. Axisymmetric elastoplastic theory was used to study the change characteristics of stress and pore water stress after the pile sinking in viscous soil, and the change rule of stress field with depth was given. Brank et al [23] studied the numerical solution of circular hole expansion based on stress-strain test curves. Tatsvnovi[24] regarded the soil plug as a series of spring units connected in series with mass points by using stress wave theory, and carried out dynamic and static mechanical analysis of the process of pile penetration. L.C. Skinner et al [25] established a mathematical model of sampling process based on the principle of soil mechanics, and analyzed the influence of the gravity coring device and the piston sampler on the disturbance of marine sediment samples. Shogaki, T et al [26] used sand to simulate soil. Through sampling experiments, the disturbance of soil by the sampler under different pipe diameters and speeds was studied, and the results showed that the soil which was 0.35~1.35mm from the tube wall was easy to be influenced by friction force and had nothing to do with the tube diameter. However, this study was based on anhydrous environment, which was different from sampling in deep-water environment.

However, due to the lack of understanding of the physical mechanism of sediment strain and stress characteristics during the coring process and many uncertainties in the sampling process, some researchers have turned to numerical methods to analyze the coring process. Chopra, M.B. et al. [27] established a time-dependent large deformation finite element consolidation analysis method. They believed that the sediment followed the revised Cambridge model, and the principle of effective stress was used to derive the large deformation finite element consolidation equations which was later applied to the simulation of the sampling process. Henke et al. [28] used the finite element analysis method to conduct a finite element simulation of the open pipe pile into the soil based on the large deformation theory, but it was impossible to simulate the change of shear stress on the interface with the change of soil strength. Randolph et al. [29] conducted a one-dimensional simplified analysis of the soil plug of the pipe pile and discussed the soil plug problem under drainage conditions, but did not consider the undrained conditions. Zhou Wen et al. [30] applied a nonlinear finite element analysis method to establish a two-dimensional axisymmetric finite element model of the sampling tube in contact with the sediment, and selected the Drucker-Prager elastoplastic model to simulate the sediment. The disturbance of sediment during the sampling process of the tubular sampler was studied. The results confirmed that sampling would cause the mingling, bending, deformation and shortening of sediment samples. But this method also ignored the effect of drainage pressure. HUAWEI QIN et al.[31] proposed a numerical method for simulating gravity coring. The sediment model used a modified Drucker-Prager constitutive model. A three-dimensional finite element model based on ABAQUS was established, and the sampling effect was analyzed using the Euler-Lagrange coupling method. This method can simulate extreme deformation, penetration and other problems, and the finite element model well-captured the obvious under-sampling phenomenon. Yuan Guo et al. [32] used the discrete element model (DEM) to simulate the clogging mechanism of the soil inside the large-diameter pipe pile, comprehensively simulating the interaction between the soil particles and the interaction between the soil particles and the pipe pile. The influence of factors such as the length of the soil column, the inner diameter of the pile, the particle size, the friction coefficient of the pile-soil interface was studied. Wegener et al. [33] studied the soil mechanics phenomena affecting the recovery of particulate soil in the tubular vibroflotation test through a literature review and a discrete element model correction of the the physical vibro flotation test results.

However, the above-mentioned theoretical analysis and numerical simulation are mostly carried out by the elastoplastic model based on the principle of soil mechanics to characterize the seabed sediments. However, there are few studies using fluid-related models to describe sediment. In addition, the influences of drainage pressure and sampling speed on coring rate and sample disturbance are ignored. To this end, this paper takes the sampling device of the mechanical hand-held sampler as the research object, simulates the soft viscous sediment on the seabed surface as non-Newtonian Herschel Bulkley viscoplastic fluids, uses the finite volume method, combines the Realizable $k-\varepsilon$ turbulence

model, and applies computational fluid mechanics software Fluent to establish a numerical model of sediment sampling under deep-sea conditions. The VOF method is used to track the multiphase flow interface. Under the condition of drainage pressure, the effects of different sampling speeds, different inner diameters of sampling tubes, and different sediment dynamic viscosities on the sampling volume and coring rate were studied. It has major guiding significance for efficient sampling of seabed sediment under ultra-deepwater.

2. Methodology

The sampling device, as an important part of the sampler, is used to collect deep-sea sediment. The sampling performance of the sampler is directly determined by the sampling quality. The sampling device is mainly composed of components such as a handle, a sampling tube, a high-pressure valve, a gas-tight piece, a piston, etc. (Fig 1); a number of through holes are evenly distributed on the top side wall of the sampling tube. The outer side of the top of the sampling tube is connected with the gas-tight piece through a thread, and the top end surface and the gas-tight piece are connected with an O-shape sealing ring to guarantee the sealing and pressure-retaining of the sediment after the sampling is completed until it is inserted into the pressure-retaining cylinder.

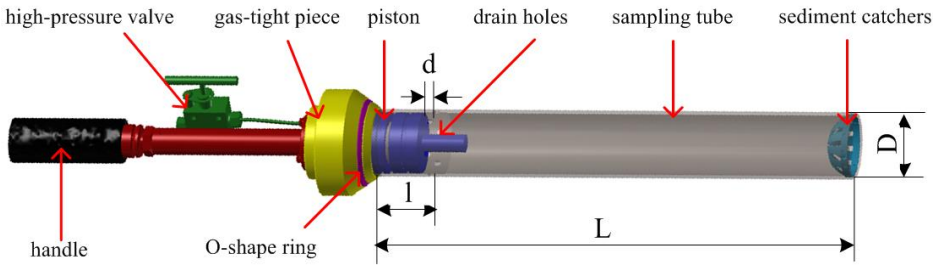

Fig 1 Structure of the sampling device

2.1 Mathematical model

It is imperative to make reasonable assumptions on the sampling model so as to simplify the model. The specific assumptions are as follows:

(1) Ignore the influence of wall thickness and catchers of the sampling tube on the sampling;

(2) During the sampling process, because the sampling speed is relatively low, it is approximately assumed that the sediment and water are not mixed with each other; in each control volume , the sum of the volume fraction of water and sediment is 1, and there is no blank area of fluid;

(3) During the sampling process of the sampling tube, the flow of sediment and water in the tube is considered to be continuous;

(4) During the removal of the sampling tube, it is approximately considered that the sediment in the sampling tube would experience no change in volume;

(5) During the experiment, the influences of temperature change and sediment moisture content change on the dynamic viscosity of the sediment is not considered.

Continuity equation:

$$\frac{1}{\rho_q}\left[\frac{\partial}{\partial t}\left(\alpha_q\rho_q\right)+\nabla\left(\alpha_q\rho_q\vec{v}_q\right)=S_{\alpha_q}+\sum_{p=1}^{n}\left(\dot{m}_{pq}-\dot{m}_{qp}\right)\right] \quad (1)$$

Where ρ_q is the physical density of phrase q; $\vec{v}_q$ is the speed of phase q; $\dot{m}_{pq}$ is the mass transfer from phase q to p; $\dot{m}_{qp}$ is the mass transfer from phase p to q; S_{α_q} is the source item, and its default value is zero.

The basic phase volume fraction is calculated from the constraint that the sum of the volume fractions of all phases is 1 without solving the volume fraction equation:

$$\sum_{q=1}^{n}\alpha_q=1 \quad (2)$$

Unit density: $\rho=\alpha_2\rho_2+\left(1-\alpha_2\right)\rho_1$, (3)

Where the seawater density is ρ_1. And in this paper, $\rho_1=1.06\times10^3\,\mathrm{kg}/m^3$ and ρ_2 is the sediment

density with $\rho_2 = 1.6 \times 10^3 \mathrm{kg}/m^3$.

Momentum equation:

By solving a single momentum equation in the entire area, the speed field obtained is shared by each phase. The momentum equation depends on the connection between the physical property parameters ρ and μ and the volume fraction:

$$\frac{\partial}{\partial \mathrm{t}}(\rho\vec{v}) + \nabla \cdot (\rho\vec{v}\vec{v}) = -\nabla p + \left[\mu\left(\nabla\vec{v} + \vec{v}^T\right)\right] + \rho\vec{g} + \vec{F} \tag{4}$$

Where μ is the hydrodynamic viscosity; $\vec{F}$ is the source item of the momentum equation caused by surface tension and wall adhesion.

$$\frac{\partial \varepsilon}{\partial \mathrm{t}} + \vec{u}_i \frac{\partial \varepsilon}{\partial x_i} = \frac{\partial}{\partial x_i}\left[\sigma_\varepsilon \mu_{eff} \frac{\partial \varepsilon}{\partial x_j}\right] + \rho c_1 S_\varepsilon - \rho c_{2\varepsilon} \frac{\varepsilon^2}{k + \sqrt{v\varepsilon}} \tag{5}$$

Where， $\mu_{eff} = \mu_1 + \mu_\mathrm{t}$； Where $\mu_{eff} = \mu_1 + \mu_\mathrm{t}$

$$c_1 = \max\left[0.43, \frac{\eta_1}{\eta_1 + 5}\right]$$

$$\eta_1 = S_\varepsilon \frac{\mathrm{k}}{\varepsilon}$$

$$S_\varepsilon = \sqrt{2S_{\mathrm{ij}}S_{ij}}$$

The Realizable $k-\varepsilon$ model is used to simulate round-mouth flow problems, including swirling uniform shear flow, free-flow pipes, boundary laminar flow, and separation flow. The model is currently widely-used in numerical calculations of various flow types.

Assuming that the insertion depth of the sampling tube into the sediment is L; the height of the sediment in the sampling tube is H, and the sampling volume is Q, then:

$$Q = \frac{1}{4}\pi D^2 H \tag{6}$$

At the same time, in order to further evaluate the sampling performance of the sampler, the concept of coring rate is introduced. The coring rate is λ:

$$\lambda = \frac{H}{L} \times 100\% \tag{7}$$

The coring rate λ is an important index of deep-sea sediment sampling equipment. The larger λ is, the better the sampling performance is; the lower λ is, the worse the sampling performance is. Therefore, how to effectively increase the coring rate of the sampler is the research focus of this paper.

2.2 Calculation domain and mesh generation

The sampling device works in an open water environment, and only a certain area of the flow field has a significant impact on the sampling process. Before the establishment of calculation model, the sampling device is simplified into a round tube with a closed upper end and an open lower end, ignoring the influence of the wall thickness and catchers of the sampling tube on the calculation model. Assuming that the sampling speed of the sampling tube is v, different speeds can be set by writing UDF programs. Considering that the location of the drain holes is not symmetrical, the model is the entire cylindrical calculation domain. The criterion to set the calculation domain size is to minimize the impact of blocking. The entire calculation domain is divided into seawater area and sediment area. The settings and parameters of the calculation domain are shown in Fig 2 and table 1:

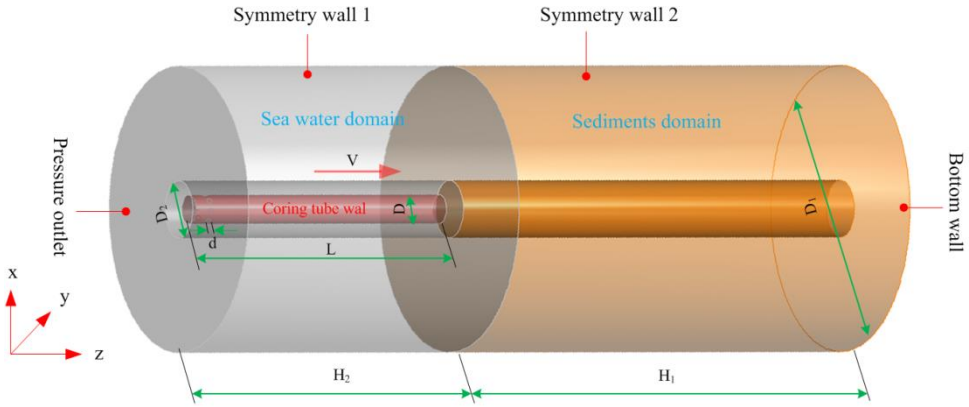

Fig 2 3D calculation model of sampling

Tab.1 Parameters of calculation model

Parameter Types	Names	numerical value
Parameters of structure	Length of samplingtube L/mm	500
	Diameter of sample tube D/mm	20~80
	Diameter of the drain holes d/mm	2~20
	Location of the drainage hole I/mm	20
parameters of the calculation model	Length of sea area H2/mm	600
	Length of sediment H1/mm	1000
	Diameter of calculation area D1/mm	500
	Radius of dynamic mesh area D2/mm	180
	Sampling speed v/(mm/s)	20~200

The quality of mesh generation directly affects the accuracy of the calculation results. In order to obtain higher calculation accuracy and reduce the quantity of calculation, the watershed is treated in a boundary layer and sub-regional manner, and the outermost layer uses a hexahedral-based mesh generation. The inner layer adopts the tetrahedron-based mesh generation. At the same time, the boundary layer mesh exists in the area where the sampling tube is in contact with the fluid, which is aimed at achieving high accuracy of the numerical calculation. The mesh model of sampling is shown in Fig 3.

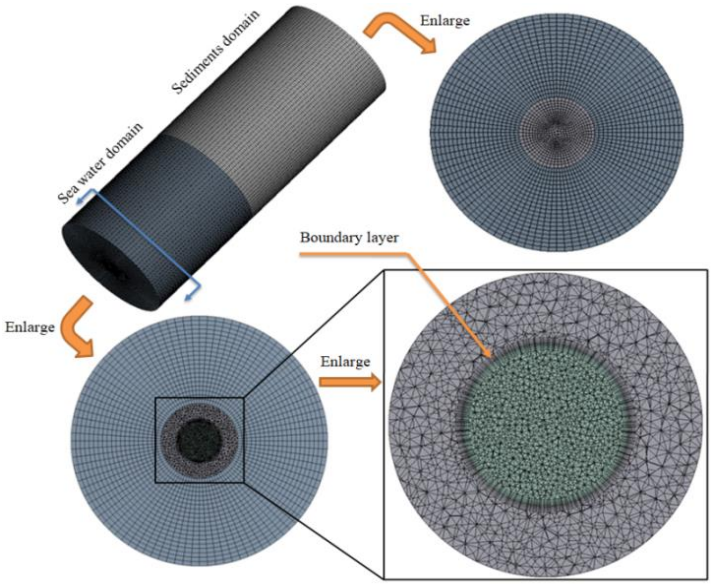

Fig 3 Mesh model of sampling

2.3. Calculation parameters and boundary conditions

2.3.1 Calculation parameters

The multi-phase flow model and the realizable k-ε turbulence model were used to simulate the flow field in the calculation domain. The calculation uses 3D single-precision, and the dynamic mesh change is controlled by a dynamic layering method, which activates the size function control to prevent excessively distorted mesh during the calculation process. The convection term is discretized by a first-order upwind scheme which is easy to converge. The pressure solver is used, and PISO algorithm is used for pressure and speed coupling.

2.3.2 Boundary Conditions

Outlet boundary condition: adopting the boundary condition of pressure exit, with gauge pressure of 0.

Wall condition: the lower boundary of the calculation domain is a fixed wall condition, and the cylindrical surface of the calculation domain adopts a symmetric boundary condition.

2.4 Settings of parameters

2.4.1 Inner diameter of the sampling tube

Laboratory sampling experiments and research data show that the sampling volume and coring rate are related to the diameter of the sampling tube. The larger the diameter of the coring device is, the better the sampling performance is. The selection of the inner diameter D of the sampling tube should first meet the index requirements of the sampling volume, and at the same time, the problem of insufficient sampling volume caused by blockage of sediment at the cutter head during sampling should also be considered. In this paper, the inner diameter d of the sampling tube is set in the range of 20 mm to 80 mm to meet the research purpose.

2.4.2 Sampling speed

The sampling efficiency of the sampler is determined by the inner diameter, inner wall roughness of the sampling tube as well as sediment characteristics. Relevant documents show that the sampling volume and coring rate are related to the sampling speed. Therefore, the selection of sampling speed should be taken into consideration. Excessive sampling speed will hinder the flow of water in the sampling tube or prevent water from being discharged, and the upper surface of sediment in the sampling tube may generate water pressure to reduce the coring rate. In order to study the influence of sampling speed on sampling volume and coring rate, the range of simulated sampling speed is set at 20 mm/s to 200 mm/s in this paper.

2.4.3 Drainage area ratio at inlet and outlet

In the actual sampling process, if the drainage in the sampling tube is not smooth or completely closed, the flow of water in the sampling tube will be blocked or cannot be discharged, and the upper surface of sediment in the sampling tube may generate water pressure to reduce the sampling rate. In order to overcome this “hydraulic effect”, drain holes with a certain diameter is arranged on the upper circumference of the sampling tube to reduce the hydrostatic pressure on the upper surface of the sediment. In this paper, it is proposed to set up several drainholes with diameter d in the upper circumference of the sampling tube, and the number and diameter of drain holes must match the structure of the sampling tube. The drainage area ratio at the inlet and outlet of the fluid in the sampling tube is introduced and is defined as follows:

$$\beta = \frac{S_{\text{in}}}{S_{out}}, \tag{8}$$

Where S_{in} is inlet area of the sampling tube, S_{out} is the outlet area of the sampling tube.

$$S_{\text{in}} = \frac{1}{4}\pi D^2 \tag{9}$$

Where D is the diameter of the sampling tube.

$$S_{in} = N \times \frac{1}{4}\pi d^2 \tag{10}$$

Where N is the number of drain holes, and take N=8; d is the diameter of drain holes.

Under the condition that the tube diameter of the sampling tube has been taken, setting $0 < \beta \leq 12$, the influence of different drainage area ratio at inlet and outlet on the sampling volume and coring rate is studied.

2.4.4 Dynamic viscosity of sediment

Relevant research data show that the sediment located on the seabed surface have high moisture content and certain viscosity, which conform to the characteristics of non-Newtonian fluid. The Herschel Bulkley model is one of the simplest viscoplastic models in non-Newtonian fluids. The model is described by the following parameters:

$$\begin{cases} \dot{\gamma} = 0, & |\tau| \leq \tau_0 \\ |\tau| = \tau_0 + K|\dot{\gamma}|^n & |\tau| > \tau_0 \end{cases} \tag{11}$$

Where τ_0 is the yield stress; $\dot{\gamma}_c$ is the critical shear rate; K is the consistent coefficient; n is the power law index. The above formula is simplified as n=1. The shear stress changes linearly with the shear strain rate, thus K is hydrodynamic viscosity η .

Because the dynamic viscosity of sediment is directly related to the moisturer content of fluid, the temperature and pressure of the environment, and the sediment in different depths and different sea areas is also different. Based on this, in the absence of specific values of sediment dynamic viscosity, this paper sets the sediment dynamic viscosity as 10^{-2}~10^{2} kg/m·s to study the influence of dynamic viscosity on sampling volume and coring rate.

3. Results and discussion

As shown in Fig 4, under the condition of known sampling tube length L, diameter D and drain hole diameter d, In the process of inserting the sampling tube, the sediment entering the tube needs to overcome its own viscous resistance, interfacial surface tension and water resistance. Therefore, when the sampling is finished, the height of sediment entering the tube can be clearly observed, and the length of sediment in the sampling tube is less than its penetration depth.

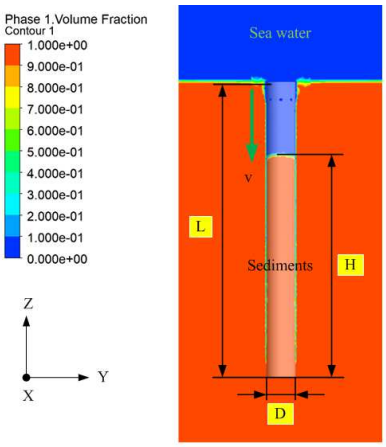

Fig 4 Schematic diagram of sampling results

In order to further study the relationship between sampling efficiency and influencing parameters, this paper calculates the influence of different sampling speeds, inner diameters of sampling tube, drainage area ratio at inlet and outlet, and dynamic viscosity of sediment on sampling volume and coring rate.

3. 1 Influence of internal diameter of sampling tube

In this section, the sensitivity of the diameter of the sampling tube is analyzed, and the influence of different inner diameters of the sampling tube on the sampling volume and coring rate is studied. On the premise of the length of the sampling tube 500 mm, the viscosity of sediment 10 kg/m·s, the diameter of drain holes 5 mm and six different speeds, the diameter ranges from 20 to 80 mm.

Fig 5 and 6 show the influence of the inner diameters of the sampling tube on the sampling volume and coring rate. It can be seen that the sampling volume increases linearly with the increase of diameter of the sampling tube. The smaller the sampling speed is, the more obvious the increasing trend of the sampling volume is. Under the same conditions, the coring rate first increases and then decreases with the increase of the diameter of the sampling tube. When the sampling speed is 200 mm/s and the diameter of the sampling tube is 40 mm, the coring rate is about 33%. When the sampling speed is 20 mm/s and the diameter of the sampling tube is 70 mm, the coring rate is around 80%. Therefore, when designing the sampling tube, increasing the diameter of the sampling tube can increase the sampling volume. However, the coring rate increases first and then decreases, which is critical for the design of the sampler with the demand on the coring rate.

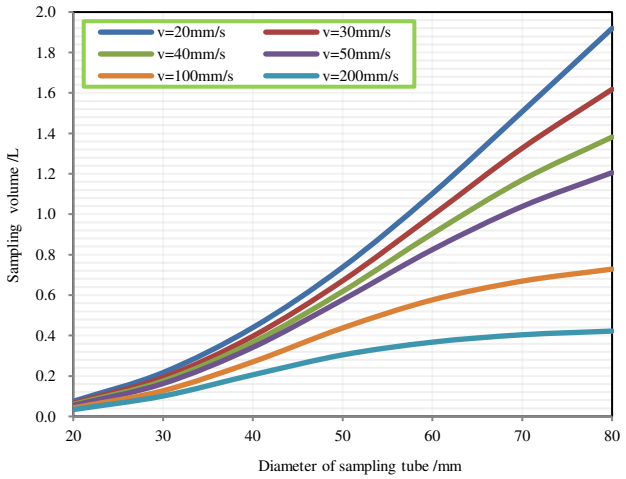

Fig 5 Relationship between sampling volume and inner diameter of sampling tube

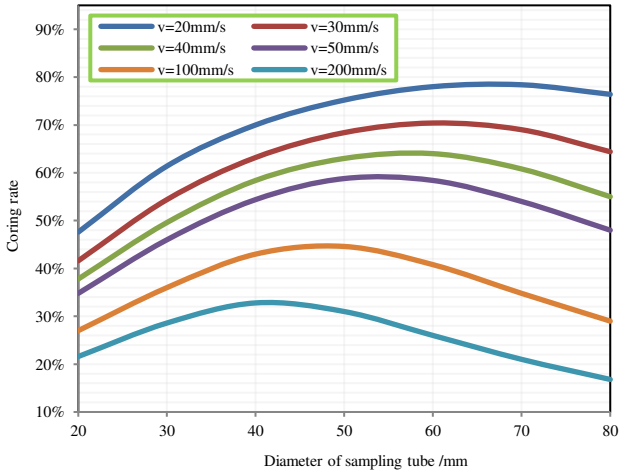

Fig 6 Relationship between coring rate and inner diameters of sampling tube

3. 2 Influence of drainage area ratio at the inlet and outlet

Different drainage area ratio at inlet and outlet determines whether the water in the sampling tube can be drained smoothly or not. Therefore, in this section, numerical simulation of drainage area ratio at inlet and outlet of 1, 2, 3, 4, 6, 8 and 12 are calculated respectively, and the influence of different drainage area ratio at inlet and outlet on sampling volume and coring rate is studied.

Fig 7 and 8 show the influence of drainage area ratio at the inlet and outlet of sampling tube on sampling volume and coring rate. Under the conditions of sampling tube length 500 mm, sediment viscosity 10 kg/m·s and sampling speed 100 mm/s, when drainage area ratio at inlet and outlet is less than or equal to 3, the sampling volume and coring rate basically remain unchanged; When the drainage area ratio at the inlet and outlet is greater than 3, the sampling volume and coring rate decrease with the increase of the drainage area ratio at the inlet and outlet. The larger the diameter of the sampling tube is, the more obvious the decreasing trend is. When the inlet area is less than or equal to 3 times of the outlet area, the drainage requirements can be met, which provides an important

reference for the design of drainage discharge of the sampler.

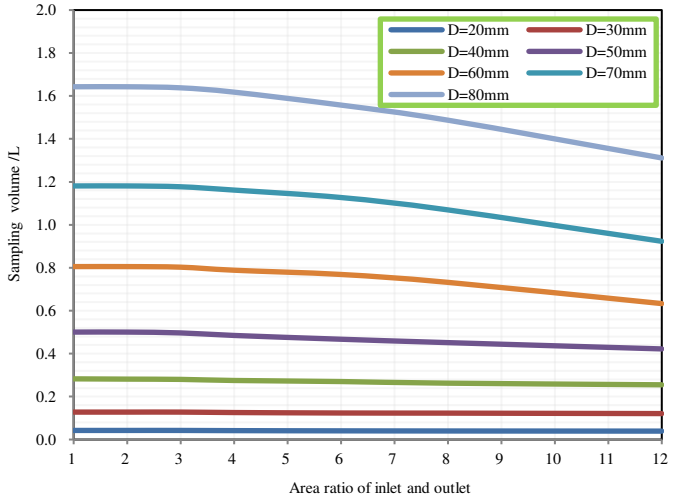

Fig 7 Relationship between sampling volume and drainage discharge

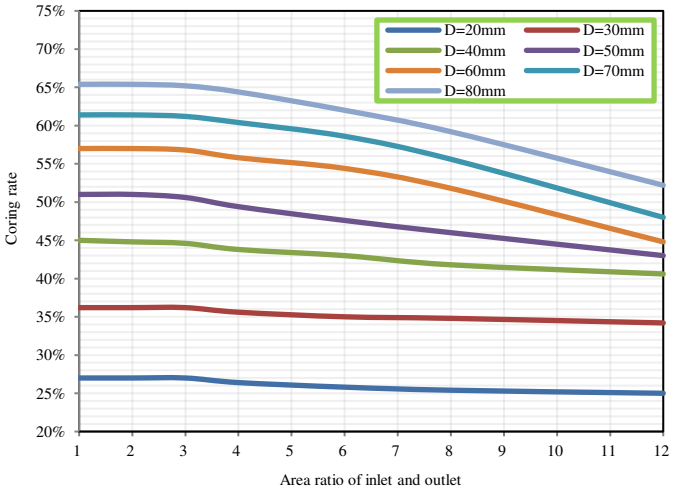

Fig 8 Relationship between coring rate and drainage discharge

3. 3 Influence of sampling speed

The sampling speed directly affects the surface tension, wall adhesion and fluid friction loss, thus affecting the amount of sediment entering the sampling tube. In response to this problem, the influence of different sampling speeds on the sampling volume and coring rate is studied in this section. Numerical simulation is carried out for the sampling speeds of 20 mm/s, 30 mm/s, 40 mm/s, 50 mm/s, 100 mm/s, and 200 mm/s respectively. Under the conditions of sampling tube length 500 mm, drain hole diameter 5 mm and sampling tube inner diameter 40 mm, the sampling volume and coring rate decrease with the increase of sampling speeds, and the smaller the sediment dynamic viscosity is, the more obvious the influence of the sampling speed on the sampling volume and coring rate is.

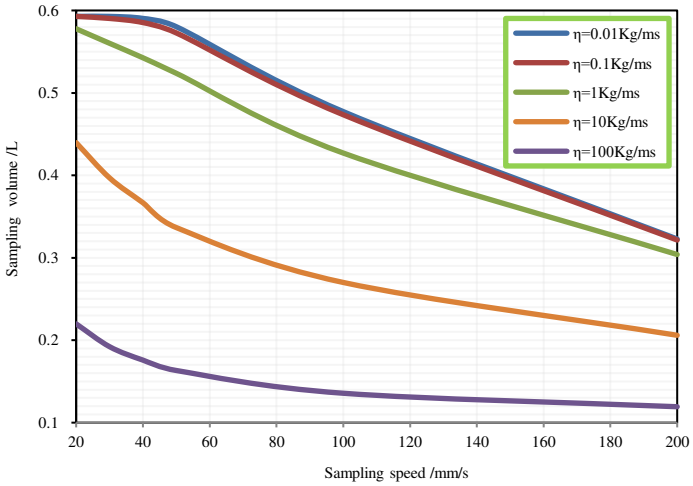

Fig 9 Relationship between the sampling volume and sampling speed

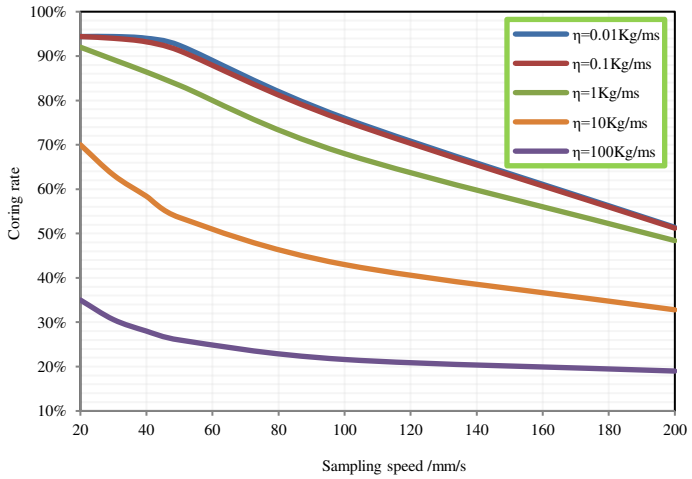

Fig 10 Relationship between the coring rate and sampling speed

3. 4 Influence of sediment dynamic viscosity

The dynamic viscosity of the sediment directly affects the surface tension of the fluid and the adhesion of the wall surface, thus determining the amount of sediment entering the sampling tube. Based on this, the influence of different sediment dynamic viscosity (0.01-100) kg/m·s on sampling volume and coring rate under different sampling speeds is studied in this section.

Fig 11 and 12 show the influence of sediment dynamic viscosity on the sampling volume and coring rate. Under the conditions of sampling tube length 500 mm, drain hole diameter 5 mm and the diameter of the sampling tube 40 mm, the sampling volume and coring rate decrease with the increase of sediment dynamic viscosity. When the viscosity is less than 0.1, the decreasing trend of sampling volume and coring rate is not obvious with the increase of viscosity. It can be seen from the figures that when the dynamic viscosity is 0.1 and 0.01, the corresponding curves of sampling volume and coring rate basically coincide. When the viscosity is greater than 0.1, the decreasing trend of sampling volume and coring rate is obvious with the increase of viscosity. Before sampling, it is necessary to measure or estimate sediment characteristic parameters such as dynamic viscosity for the design of structural parameters of the sampler.

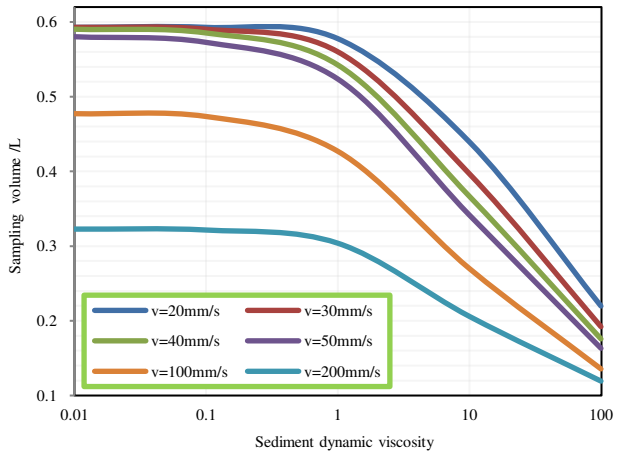

Fig11 Relationship between the sampling volume and sediment viscosity

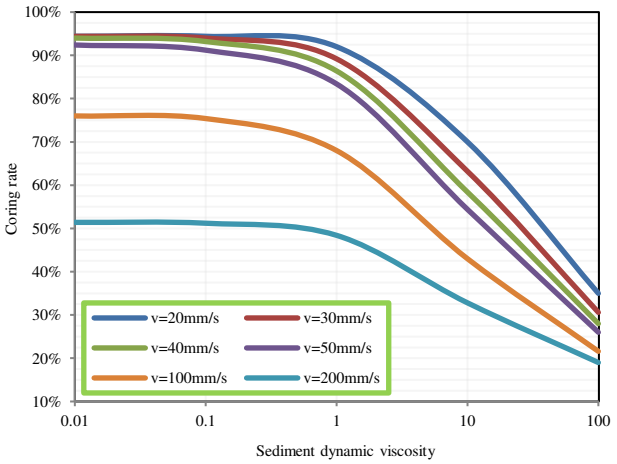

Fig 12 Relationship between the coring rate and sediment viscosity

4. Experimental study

In order to verify the correctness of the model and the results, first of all, the dynamic viscosity of the simulated sediment used in the experiment (the actual sediment taken from the seabed of the "Hainiu" drilling rig is measured by viscometer. Fig 13(a) shows the curves of the dynamic viscosity of the sediment with the change of time under several different temperature conditions. As can be seen from Fig 13(b), the dynamic viscosity of the sediment increases with the increase of temperature. And the dynamic viscosity of the sample changes rapidly and finally tends to stabilize with the increase of test time. The ambient temperature in the laboratory for this sampling experiment is about 25℃. According to the curves, the viscosity value of the experimental sample is about 80 kg/m·s after it is stable. At the same time, according to the simulation results, when the drainage area at the inlet and outlet is less than or equal to 3 in the water environment, smooth drainage can be ensured, thus ignoring the influence of drainage pressure. Since the order of magnitude of the dynamic viscosity of air is 10^{-5}, which is much smaller than that of water which is 10^{-3}, so it is feasible in principle to use laboratory air environment to replace water environment for sampling experiments under the condition that the drainage area at the inlet and outlet is less than or equal to 3. Finally, a sampling experiment platform is set up for sampling experiments.

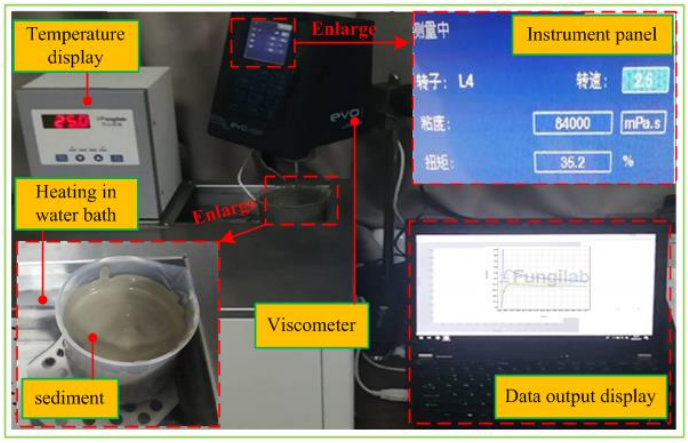

(a) Principle of measurement of experimental data

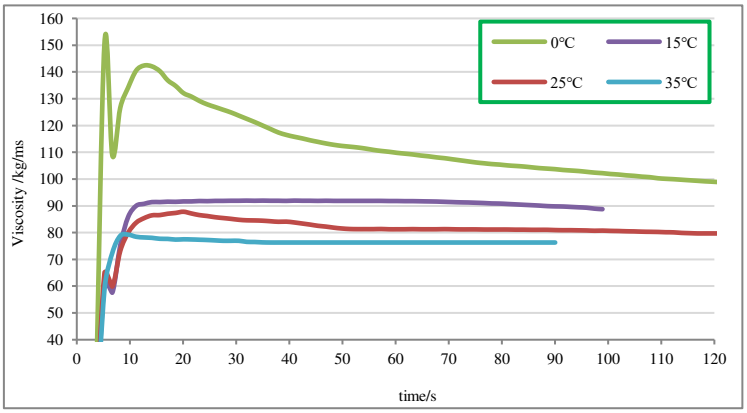

(b) Experimental data

Fig13 Determination of dynamic viscosity of sediment

4.1 Experimental principle

Through simulation analysis, the influence of various influencing factors on the sampling volume and coring rate of the sampler are obtained. According to this, taking the sampling process of the sampler as the experimental object, under the condition of known sediment dynamic viscosity, the actual sampling volumes and coring rates under specific conditions are obtained by setting different sampling speeds and different tube diameters for sampling experiments.

4.2 Construction of an experimental platform

A sampling experimental platform is set up. The simulation platform is shown in Fig 14 as follows: it mainly includes the platform body, a mud tank, an operation platform, control components and connecting pipelines. The platform body comprises a base, a circular hydraulic oil cylinder, a displacement sensor, a proximity switch, a sampling assembly fixing seat and so on; the control components include speed control buttons, a hydraulic oil tank, a three-phase motor, a pressure gauge, etc. The operation platform comprises an operation cabinet body, a touch screen (data acquisition software) and relevant operation buttons; the sampling assembly comprises a transparent sampling tube and a piston, and a sealing ring is arranged between the piston and the sampling tube.

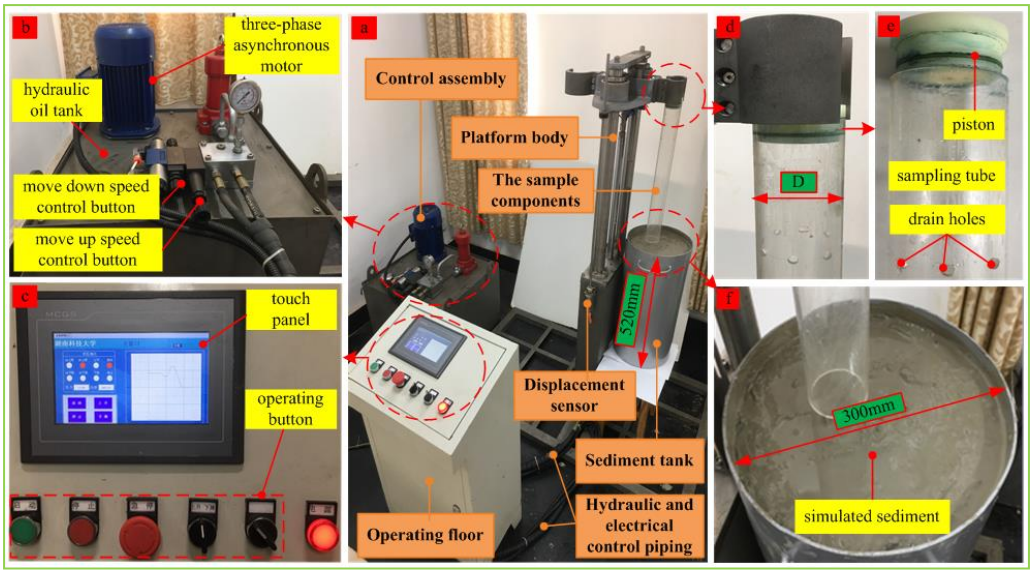

Fig14 Design diagram of the experimental platform

4.3 Experimental Procedures

The specific operation steps of the experiment are as follows:

(1) Transfer the actual sediment taken from the seabed by the "Hainiu" drilling rig to the sediment tank, and add appropriate amount of water to make the sediment in a state close to the seabed, as shown in Fig 14(f);

(2) Pre-experiment: check whether the displacement sensor is installed as required, and check whether the data acquisition software reads correctly;

(3) In order to facilitate sampling observation and measurement of experimental data, a transparent circular tube with a certain thickness is used to replace the sampling tube in this experiment. The specific size is shown in Fig 15. Install the sampling assembly with inner diameter D1=40 mm, drain hole diameter 8 mm and length 500 mm on the clamping device so that the transparent circular tube is vertically downward, as shown in Fig 14(d);

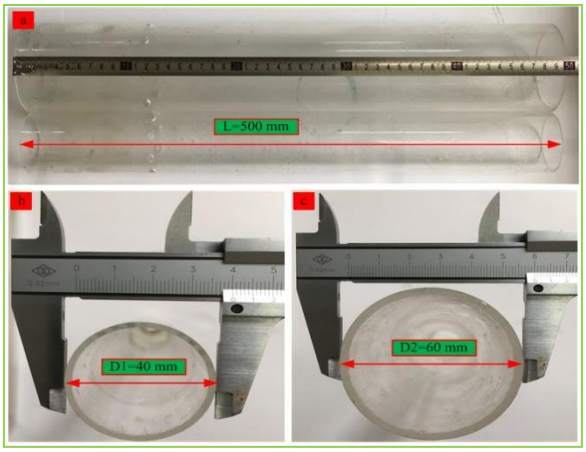

Fig 15 Size of the transparent circular tube

(4) Adjust the sampling speed and conduct the sampling experiments under the working conditions of sampling speeds of about 20 mm/s, 40 mm/s, 50 mm/s and 100 mm/s respectively. The measurement principle of experimental data is shown in Fig 16. When the sampling tube is inserted into the sediment depth of 500 mm at different speeds, to measure the height of the sediment entering the sample, only the height (Ha)from the upper end of the sampling tube to the upper surface of the sediment needs to be measured. During the experiment, when the sampling tube is inserted to a specified depth (H=500 mm), as shown in Fig 17(a), loosen the clamping device and remove the top piston as shown in Fig 17(b,c), measure the value of Ha, as shown in Fig 17(d), so that the sediment height entering the sampling tube can be calculated (Ht=500-Ha), and the experimental data (Ht)can

be recorded.

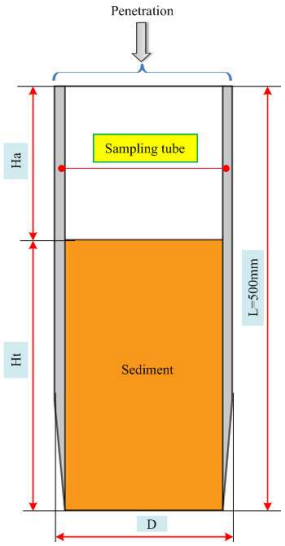

Fig 16 Measurement principle of experimental data

Fig 17 Field experiment and data measurement

(5) Install a sampling tube with inner diameter D2= 60 mm, drain hole diameter 12 mm, and length of 500 mm on the clamping device so that the sampling tube is vertically downward;

(6) Repeat the operation shown in step (4).

4.4 Experimental results

Under the conditions of tube diameters 40 mm and 60 mm, sampling experiments at different speeds are respectively carried out to obtain the height of sediment (Ht) in the sampling tube, and the corresponding sampling volumes and coring rates are calculated from this. The experimental results are shown in table 2: Ht in the table is the experimental value of the sediment height in the sampling tube; Hs is the simulated calculation value of the sediment height in the sampling tube, and the final column is the relative error between the experimental results and the calculation results based on the calculation results.

Tab.2 Experimental results

Number	1	2	3	4	5	6	7	8
D/(mm)	40				60			
v/(mm/s)	20	40	50	100	20	40	50	100
H_s /(mm)	198	150	136	118	240	190	180	152
H_t /(mm)	192	155	140	113	230	196	172	145
Error	-3.0%	3.3%	2.9%	-4.2%	-4.2%	3.2%	-4.4%	-4.6%

In order to compare the experimental results with the simulation results more clearly, the following curves are made: in Fig 18, the blue curve is the simulation calculation results, and the red curve is the experimental results where (a) is the relationship between sampling volumes and sampling speeds, and (b) is the relationship between coring rates and sampling speeds when D1= 40 mm. When D2= 60 mm,(c) is the relationship between sampling volumes and sampling speeds, and (d) is the relationship between coring rates and sampling speeds.

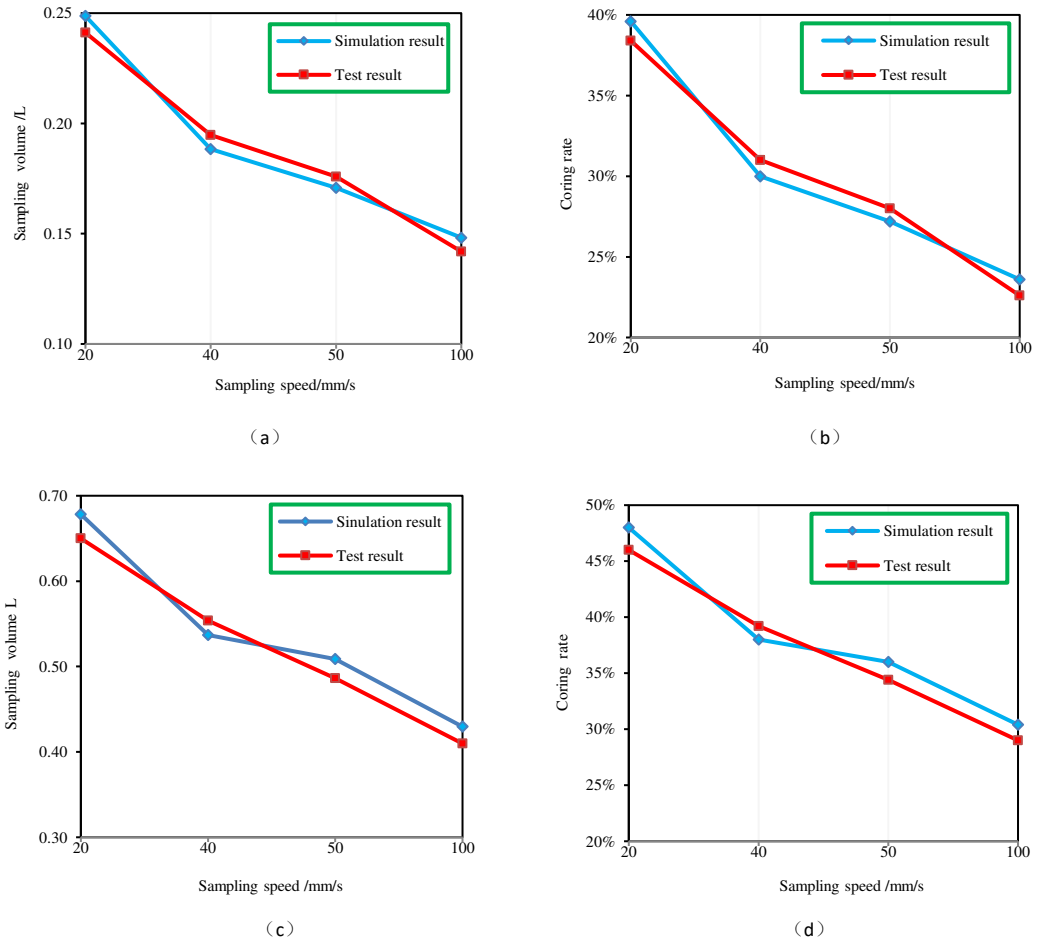

Fig 18 Comparison of simulation results and experimental results

From the experimental results, it can be concluded that the simulation results tally with the experimental results, with the maximum error being only -4.6%, and the simulation results basically coincide with the experimental results. This shows that the sediment sampling model established in this paper is reliable and the simulation results are also valid and correct.

Due to the limitations of the experimental equipment, there is no way to accurately control the sampling speed, and the dynamic viscosity of sediment will also change with the changes of sediment moisture content and laboratory ambient temperature. Meanwhile, due to the difficulty in obtaining deep-sea sediment, the sediment samples used in this experiment are not enough to form sediment areas with large diameters and deep depths, which will inevitably lead to some errors between the simulation results and the experimental results

5. Conclusions

In this paper, the sampling device of the full-ocean-depth mechanical hand-held sampler is taken as the research object; the soft viscous sediment on the seabed surface is simulated as non-Newtonian Herschel Bulkley viscoplastic fluid; the sediment sampling numerical model of the sampling device under the deep-sea condition is established; the influence of various influencing factors on the coring rates and the sampling volumes is studied, and the experimental verification is carried out, and the following conclusions are obtained:

(1) The sampling volume decreases with the increase of inner diameter of sampling tube, sampling speed, drainage area ratio at inlet and outlet and dynamic viscosity of sediment; the coring rate decreases with the increase of sampling speed, drainage area ratio at inlet and outlet, and dynamic viscosity of sediment. The coring rate first increases and then decreases with the increase of the inner diameter of sampling tube, and the peak value is related to sampling speed and tube diameter.

(2) When the drainage area ratio at the inlet and outlet is less than or equal to 3, the sampling volume and coring rate remain basically unchanged; when the drainage area ratio at the inlet and

outlet is greater than 3, the sampling volume and coring rate decrease with the increase of the drainage area ratio at the inlet and outlet. The larger the diameter of the sampling tube is, the more obvious the decreasing trend is, which provides an important reference for the design of the drainage discharge of the sampler.

(3) A sampling experimental platform is set up and experiments are carried out. The simulation results tally with the experimental results. The correctness of the model and simulation results are further verified within the allowable error range.

(4) The established simulation model and simulation results have certain reference for the design and research of the sampling device of the columnar sampler.

6. Declaration

Acknowledgements

The author sincerely thanks to Professor Deshun Liu of Hunan University of Science and technology for his critical discussion and reading during manuscript preparation.

Funding

Supported by by National Key R&D Program of China (Grant no. 2016YFC0300502), and Hunan Provincial Innovation Foundation For Postgraduate (Grant no. CX2018B658), and the National Natural Science Foundation of China (Grant no.51705145, 517779092). This work is supported by Scientific Research Fund of Hunan Provincial Education Department (Grant no.18 B205) and Hunan Province Natural Science Foundation (Grant no.2019 JJ50182).

Availability of data and materials

The datasets supporting the conclusions of this article are included within the article.

Authors' contributions

The author' contributions are as follows: Youduo Peng was in charge of the whole manuscript; Shudong He wrote the manuscript; Yongping Jin assisted in data collection. Buyan Wan provided ideas on manuscript writing.

Competing interests

The authors declare no competing financial interests.

Consent for publication

Not applicable

Ethics approval and consent to participate

Not applicable

Reference

[1] RAHUL S. Deep sea mining economic, technical, technological, and ambient considerations for sustainable development. Marine Technology Society Journal. 2017, 5(5): 28-41.

[2] Sharma R. Deep-Sea mining: Economic, Technical, Technological, and Environmental Considerations for Sustainable Development. Mar.technol.soc.j.2011, 45(45):28-41.

[3] JIN S C. Deep ocean mining technology III developments. Proceedings of the Eighth International Society of Offshore and Polar Engineers Ocean mining Symposium, September20-24, 2009, Chennai, India, 2009: 1-7.

[4]Mogg, A. O. M., Attard, K. M., et al. The influence of coring method on the preservation of sedimentary and biogeochemical features when sampling soft-bottom, shallow coastal environments. Limnology and Oceanography: Methods. 2017,15(11):905–915.

[5]Dueck, Y.,Lorke, A., et al. Laboratory and field investigations on freeze and gravity core sampling and assessment of coring disturbances with implications on gas bubble characterization. Limnolgy and Oceanography Methods. 2019,17 (11): 585-606.

[6]Emery, K.O., Dietz, R.S.. Gravity coring instrument and mechanics of sediment coring. Bull. Geol. Soc. Am. 1941, 52:1685-1714.

[7]Lebel, J., Silverberg, N., et al. Gravity core shortening and pore water chemical gradients. Deep-Sea Res. 1982,29:1365-1372.
[8]Parker, W.R., Sills, G.C.. Observation of corer penetration and sample entry during gravity coring. Mar. Geophys.Res. 1990,12:101-107.
[9]Paik, K., Lee, S.. Behaviour of soil plugs in open-ended model piles driven into sands. Mar. Georesourc. Geotechnol. 1993,11:353-373.
[10]McCoy, F.W..Photographic analysis of coring. Mar.Geol. 1980,38: 263-282.
[11]Ross, D.A., Riedel, W.R., 1967. Comparison of upper parts of some piston cores with simultaneously collected open-barrelcores. Deep-Sea Res. 1967,14:285-294.
[12]Rongve, D.,Erlandsen, A. H.. Shortening of surface sediment cores during sampling. Hydrobiologia, 1979,65(3):283–287.
[13]Jensen, P.. Meiofauna abundance and vertical zonationin a sublittoral soft bottom, with a test of the haps corer. Mar. Biol. 1983,74: 319–326.
[14]Leonard, R.. An assessment of sediment loss and distortion at the top of short gravity cores. Sediment Geol.1990, 66:57–63.
[15]Glew, J. R., J. P. Smol, and W. M. Last.. Sediment Core Collection and Extrusion, In Last W. M. and J. P.Smol, Tracking environmental change using lake sediments. 2001, 73-105.
[16]Taft, R. A., and C. Jones. Sediment sampling guide and methodologies. State of Ohio Environmental Protection Agency. 2001.
[17]Glew, J. R., J. P. Smol, and W. M. Last. Sediment Core Collection and Extrusion, In Last W. M. and J. P.Smol, Tracking environmental change using lake sediments,2001, 73-105.
[18]Smith, D. G.. Vibra coring: A new method for coring deep-lakes. Palaeogeogr. Palaeoclimatol. Palaeoecol. 1998,140:433–440.
[19]Chaney, R. C., G. Almagor. Seafloor Processes and Geotechnology, 1st Edition. CRC Press. 2015.
[20]Meyerhof, G.G.. Bearing capacity and settlement of pile foundations. Proc. ASCE, J. Soil Mech.Found. Div. 1976,102:197-228.
[21]Durgunoglu, H .T. et al. Static penetration resistance of soils Analysis. In-situ Measurment of soil properties,1975,1.
[22] Carter, J .P, Randolph, M.F.,et al. Stress and pore pressure changes in clay during and after expansion of a cylindrical carity.lnt. J.Numer. Analyst. Mech. Geomech. 1979,3 (3).
[23] Brank L, Adolfo F.,A numerical solution of cavity expansion problem in sand based directly on experimental stress-strain curves. Canadian Geotechnical Journal. 1998,35(4).
[24]Tatsvnovi,et al. Effects of plug on behavior of driven pipe piles. Soil and Foundation. 1991,31 (2).
[25] Skinner, L. C., I. N. McCave. Analysis and modelling of gravity- and piston coring based on soil mechanics. Mar. Geol. 2003.199: 181–204.
[26]Shogaki, T.. Mechanism of sample disturbance caused by tube penetration: Model tests on Toyoura sand. Soils and Foundations, 2017,57(4):527–542.
[27] Chopra, M. B., et al. Finite-element analysis of time-dependent large deformation problems. lnt. for Numer. Analyst. Mesh. Geomech, 1992,16.
[28] Henke, S. and J. Grabe.. Numerical investigation of soil plugging inside open-ended piles with respect to the installation method. Acta Geotechnica 2008,3: 215–223.
[29] Randolph M F. et al. One-dimensional analysis of soil plugs in pipe piles. Geotechnique. 1991,41 (2).
[30]Wen Zhou, Hua-wei Qin, Chen Ying. Finite element analysis of sediment sampling disturbance in the seabed. Marine science. 2009,33(12).
[31] Qin, H., Cai, Z., Hu, H., Wang, J., Ye, W., & Chen, Y.. Numerical Analysis of Gravity Coring Using Coupled Eulerian-Lagrangian Method and a New Corer. Marine Georesources& Geotechnology, 2014,34(5): 403–408.

[32] Guo, Y., Yu, X. (Bill).Soil Plugging Mechanism on Large Diameter Pipe Piles: Insight from Discrete Element Simulations. IFCEE 2015.
[33] Wegener, S. B. ; Kalumba, D.,Discrete element analysis of granular soil recovery in a vibrocore, 1st Southern African Geotechnical Conference.169-175,2016,, Sun City, SOUTH AFRICA.

Figures

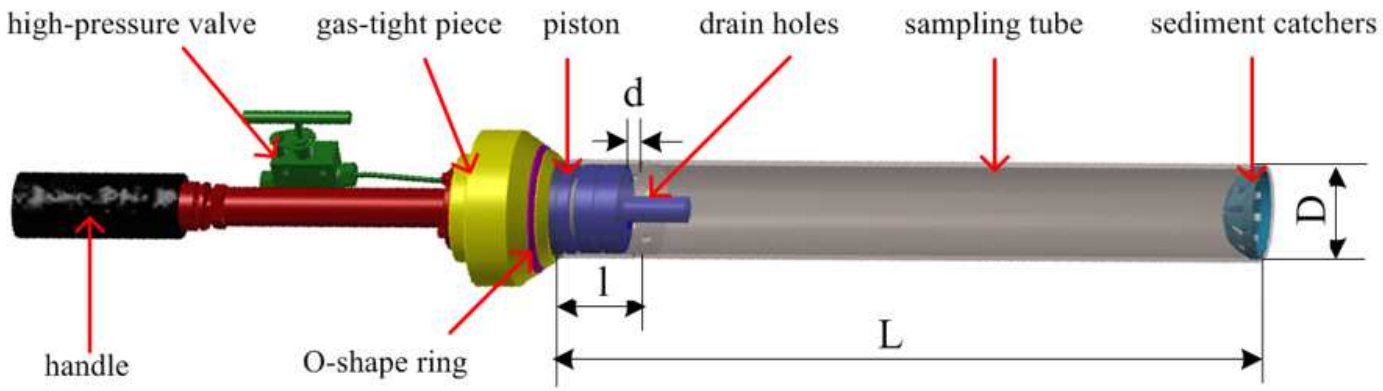

Figure 1

Structure of the sampling device

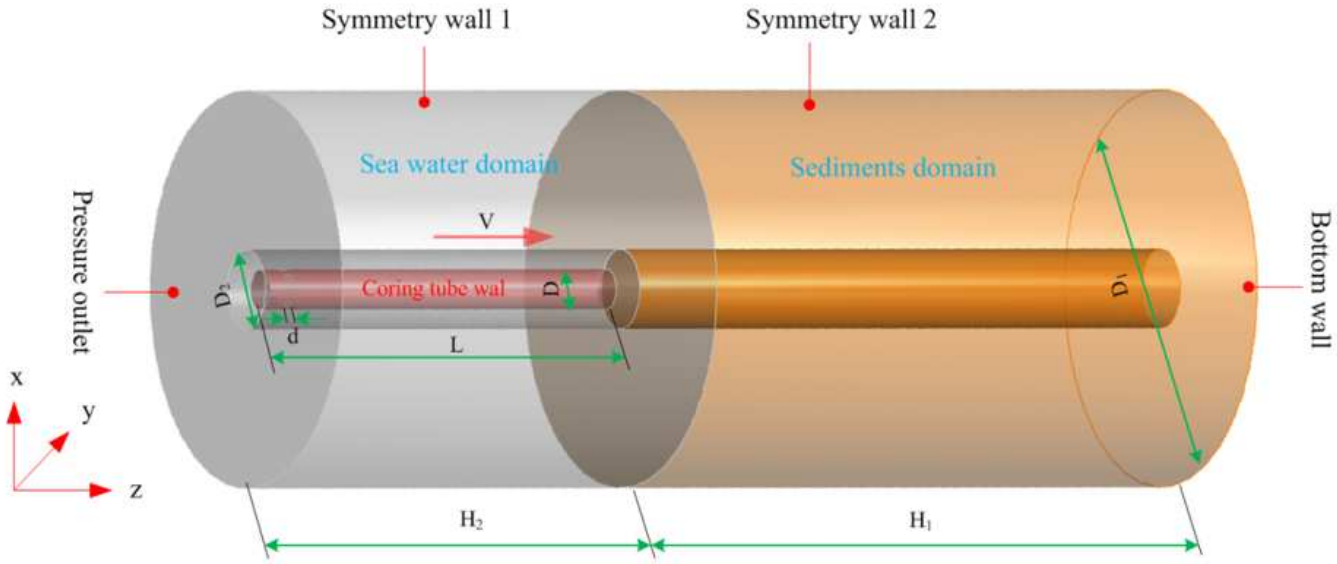

Figure 2

3D calculation model of samplin

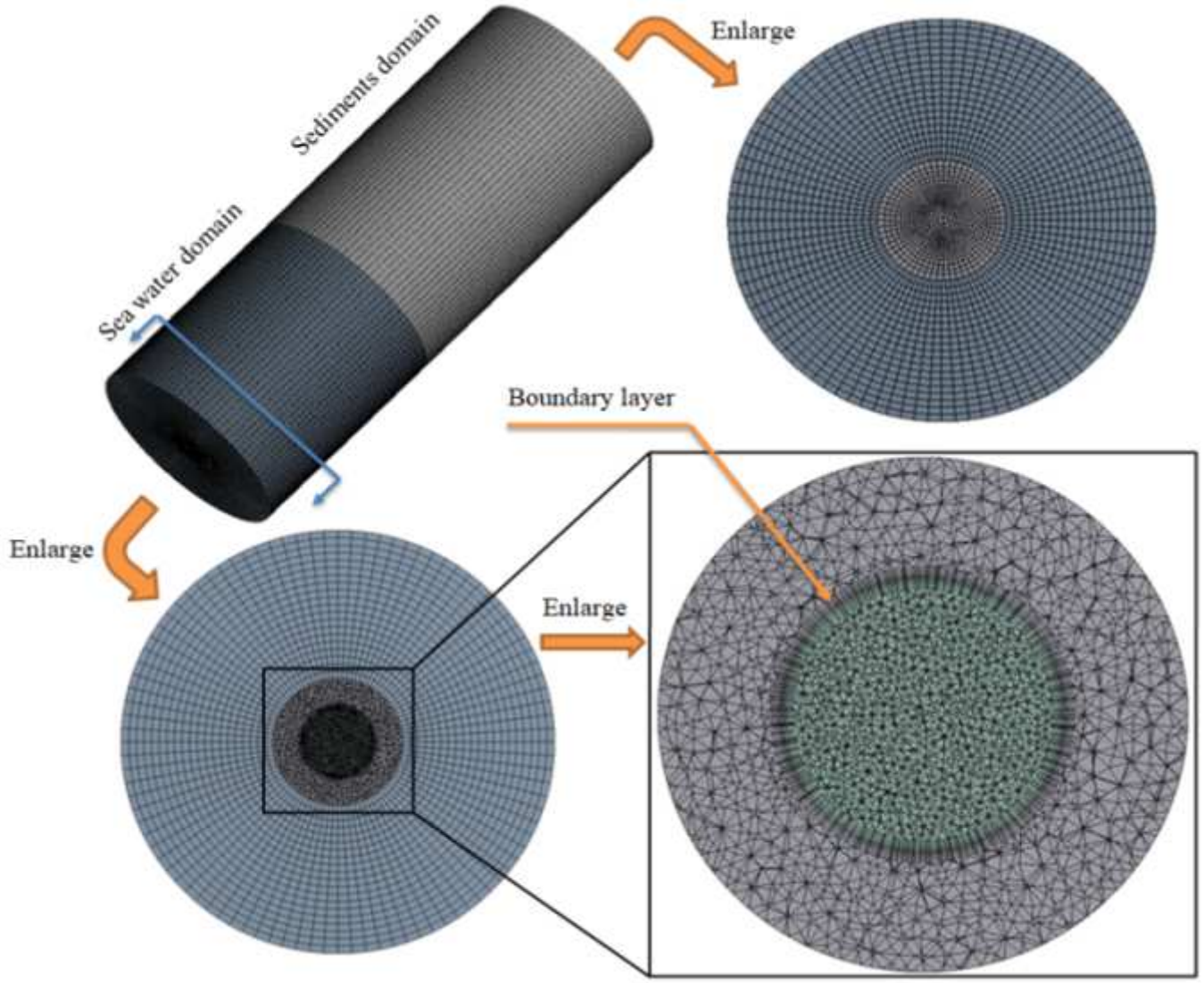

Figure 3

Mesh model of samplin

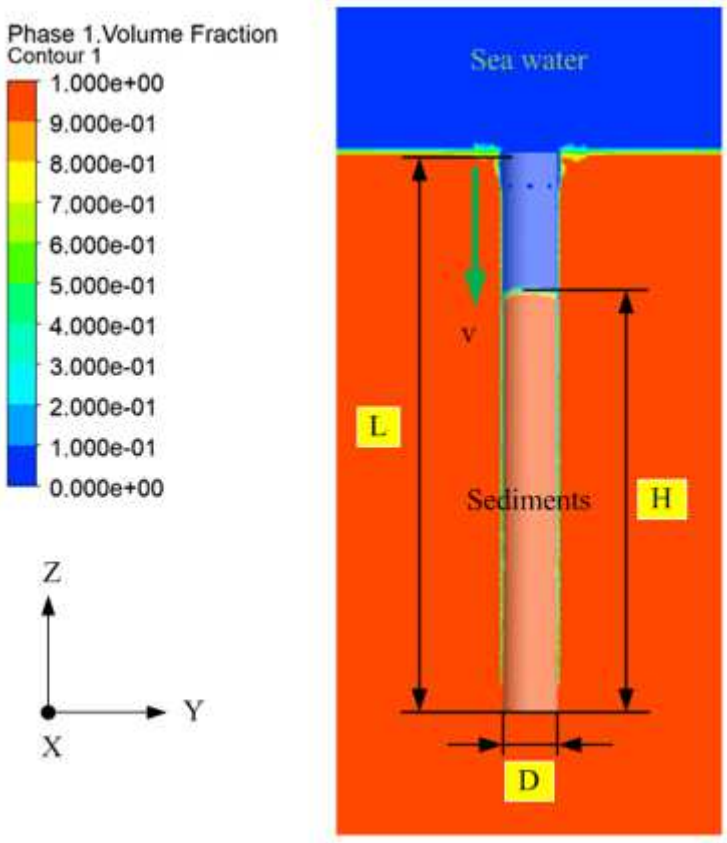

Figure 4

Schematic diagram of sampling results

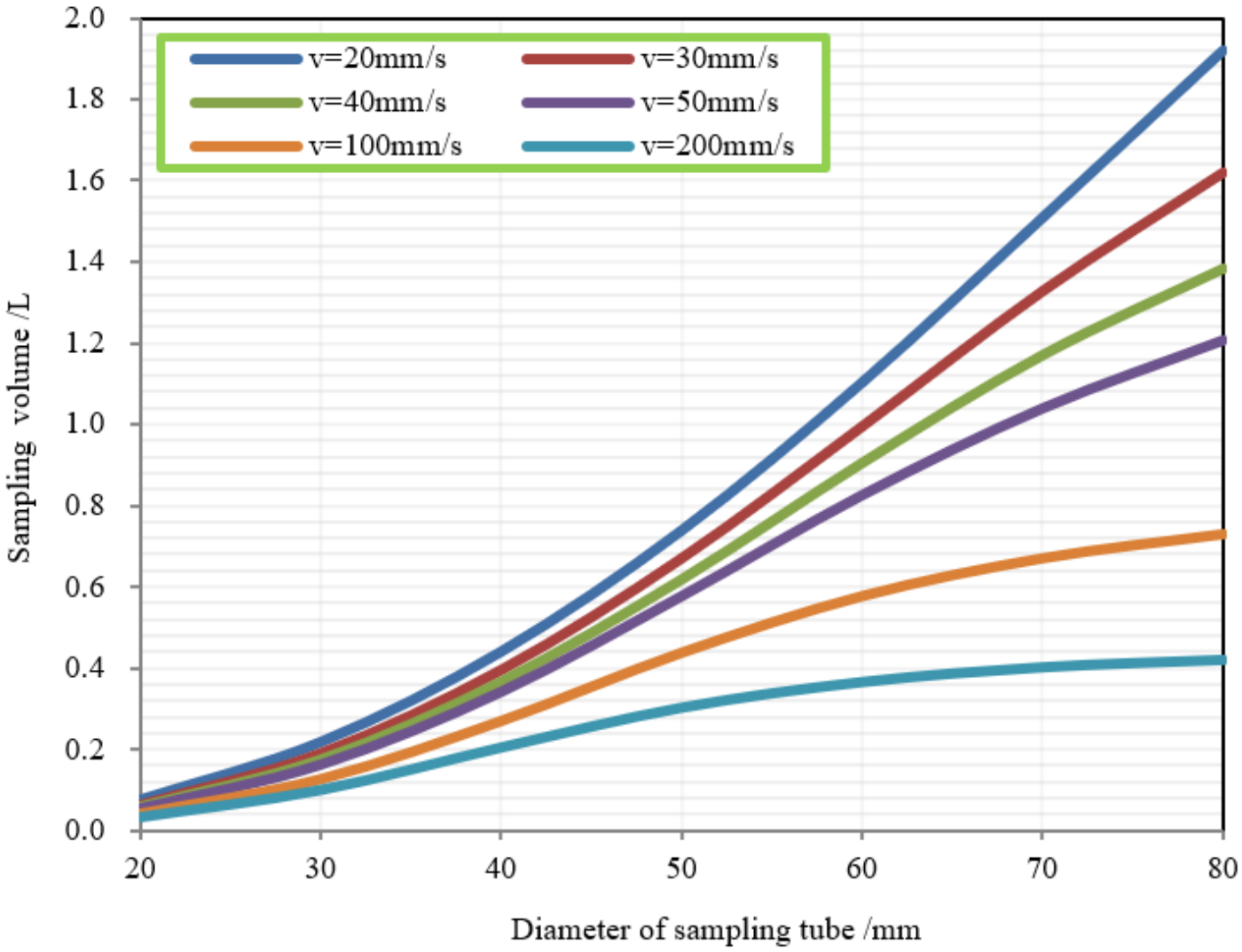

Figure 5

Relationship between sampling volume and inner diameter of sampling tube

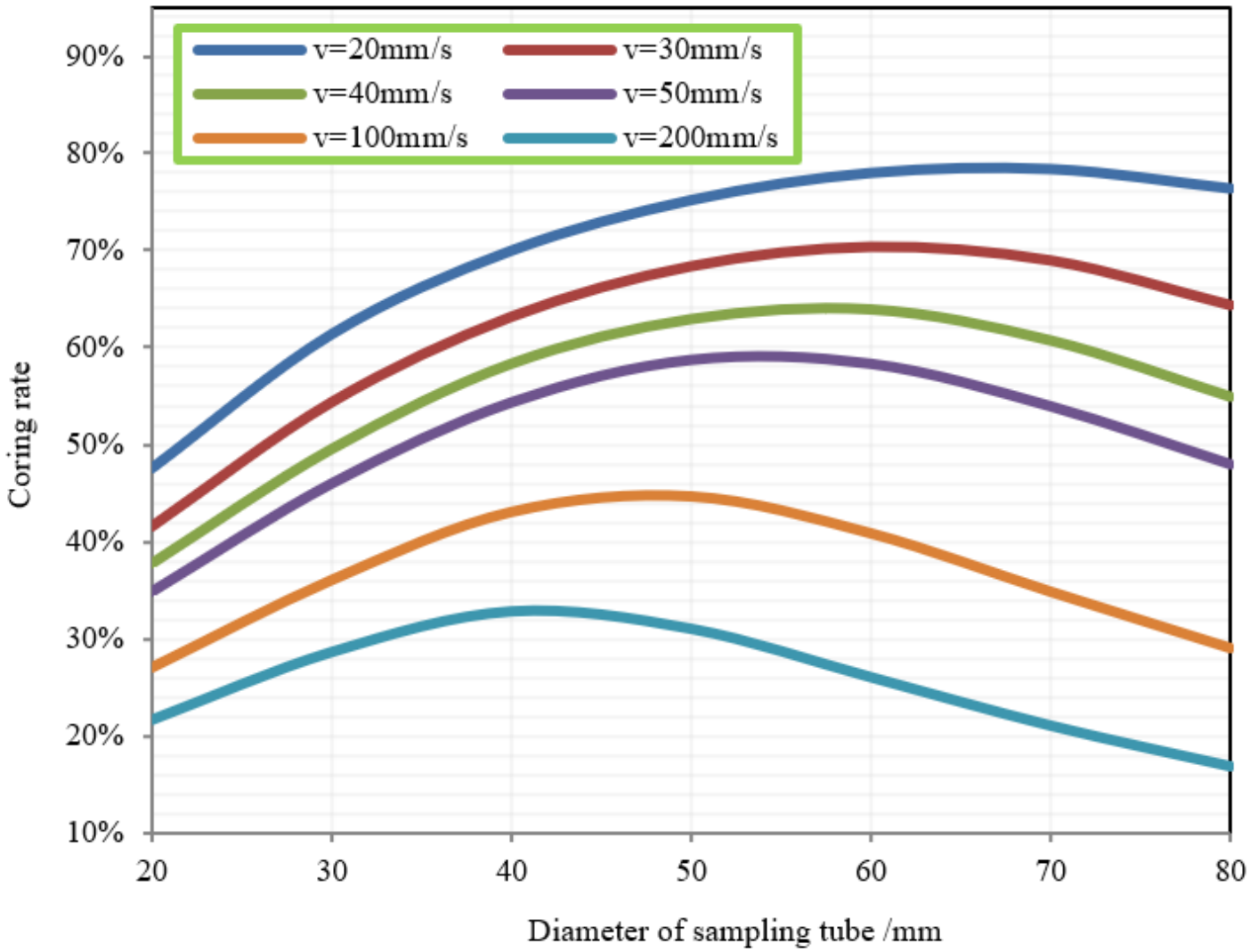

Figure 6

Relationship between coring rate and inner diameters of sampling tube

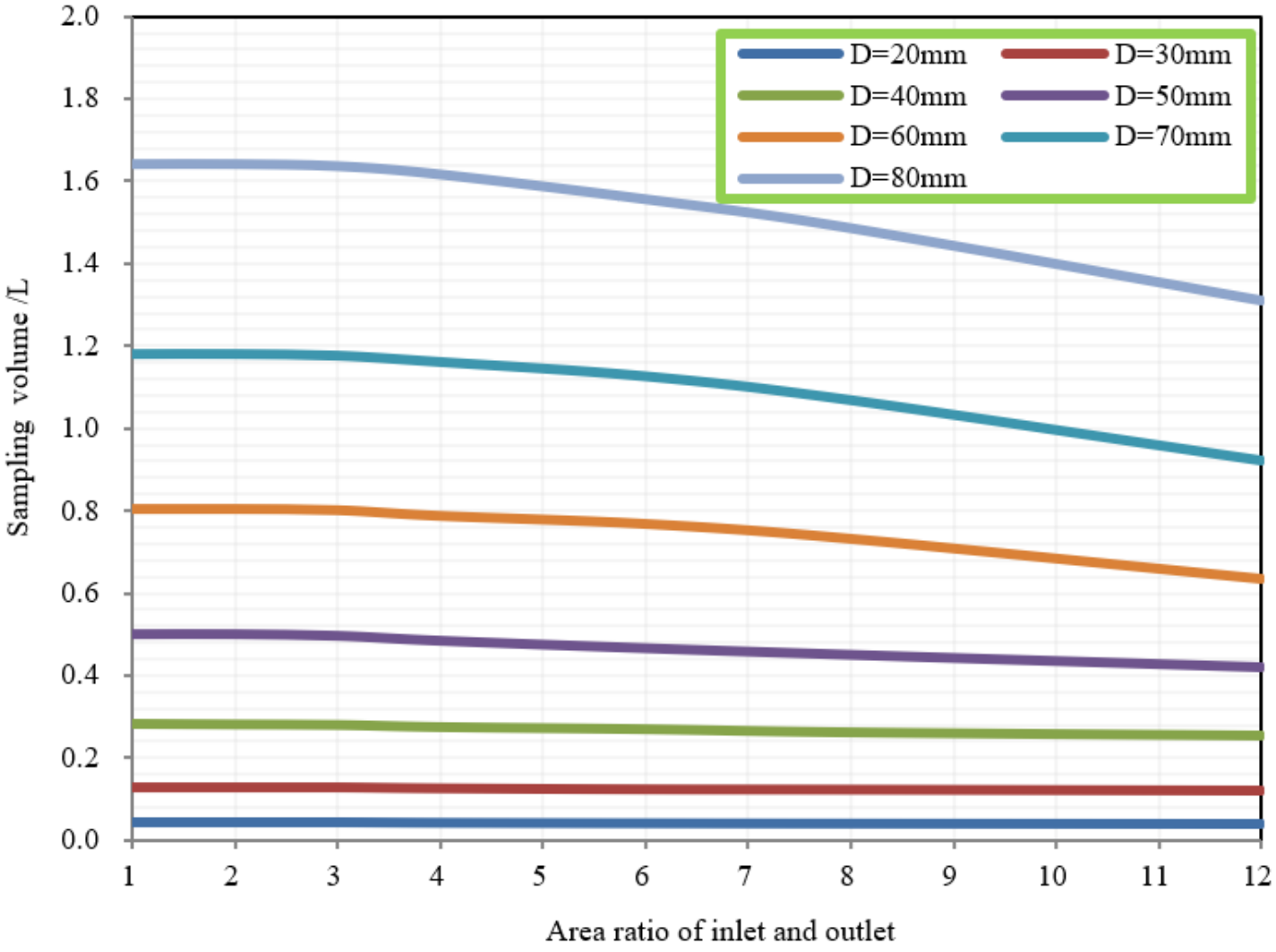

Figure 7

Relationship between sampling volume and drainage discharge

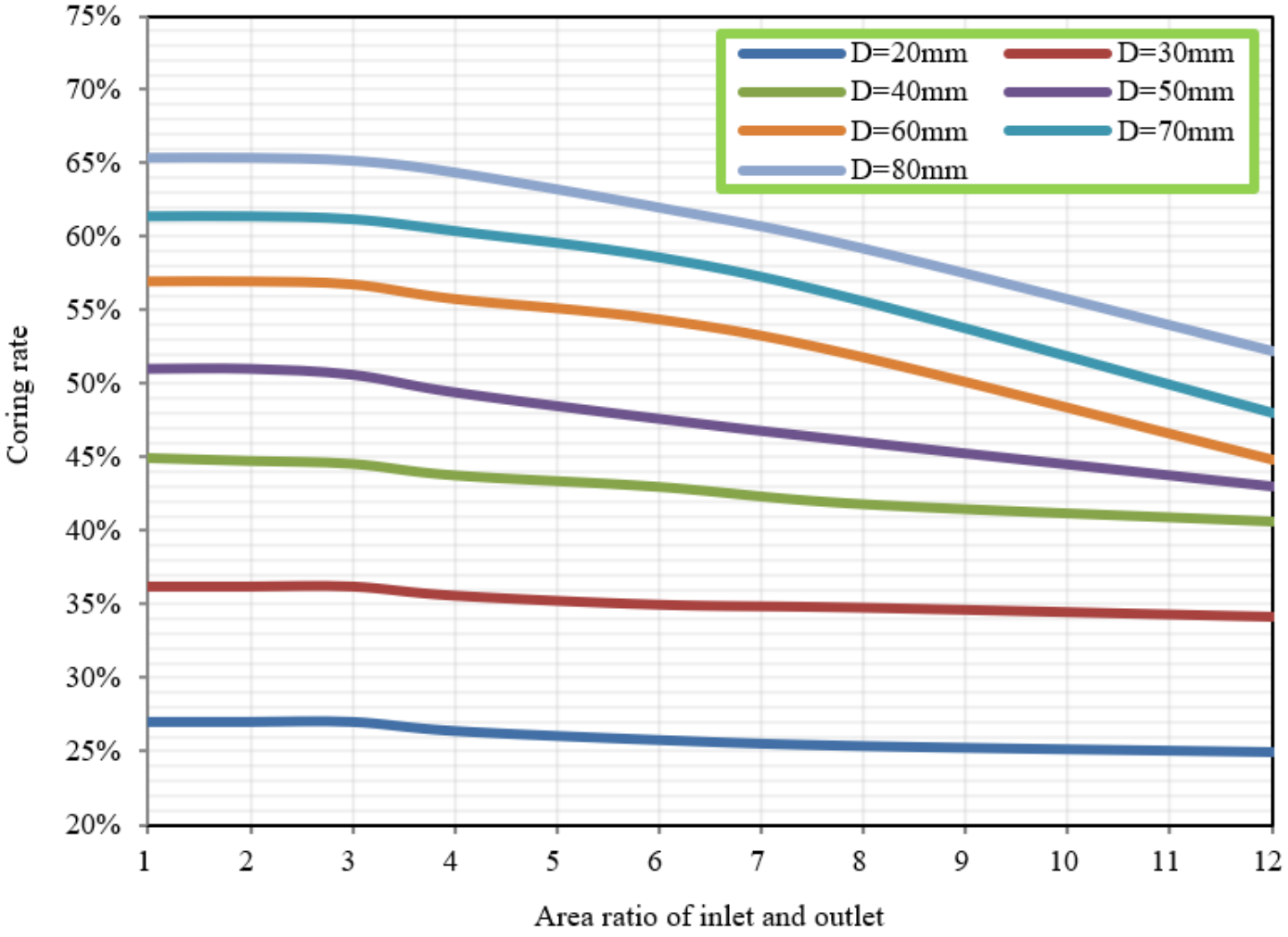

Figure 8

Relationship between coring rate and drainage discharge

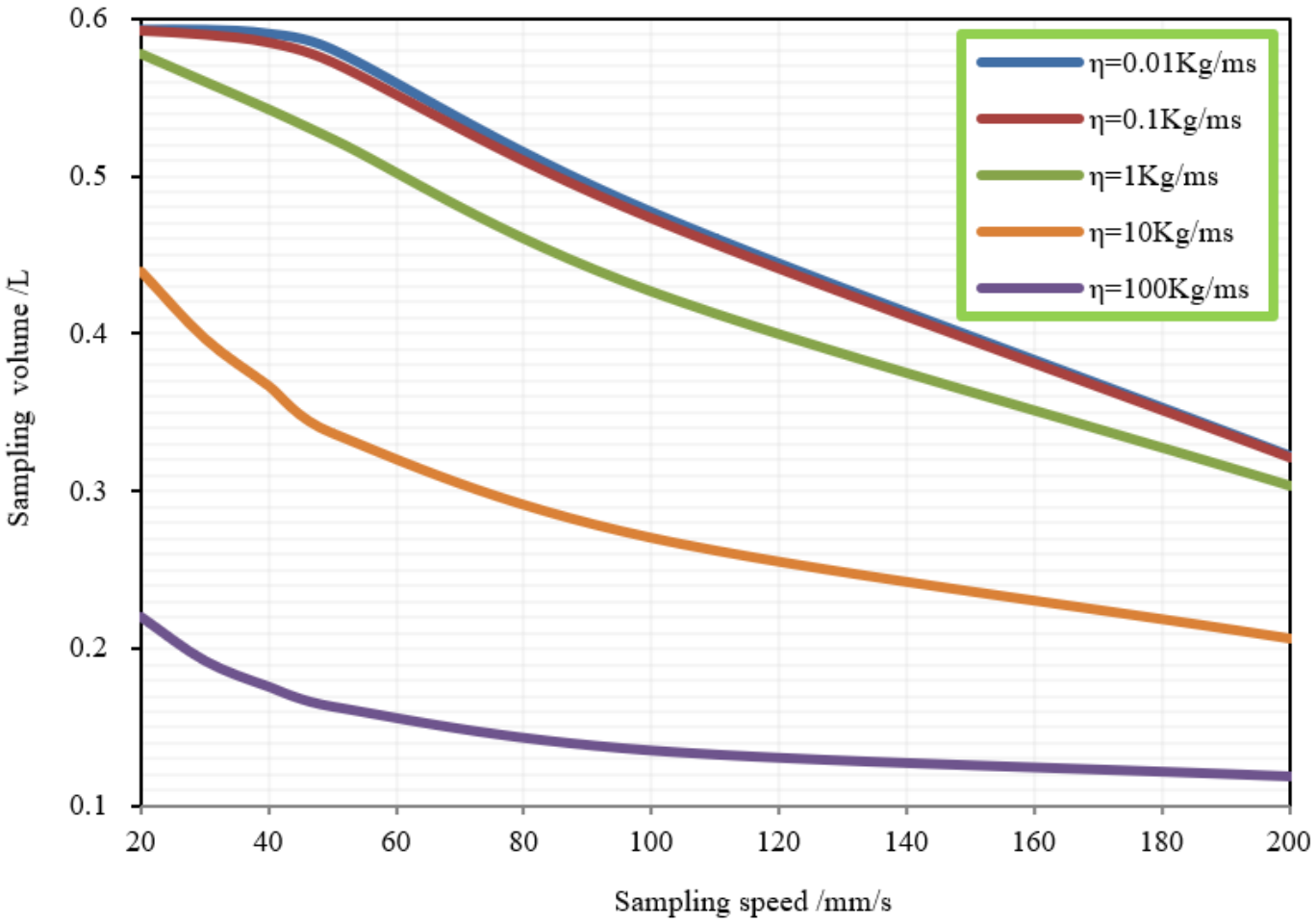

Figure 9

Relationship between the sampling volume and sampling speed

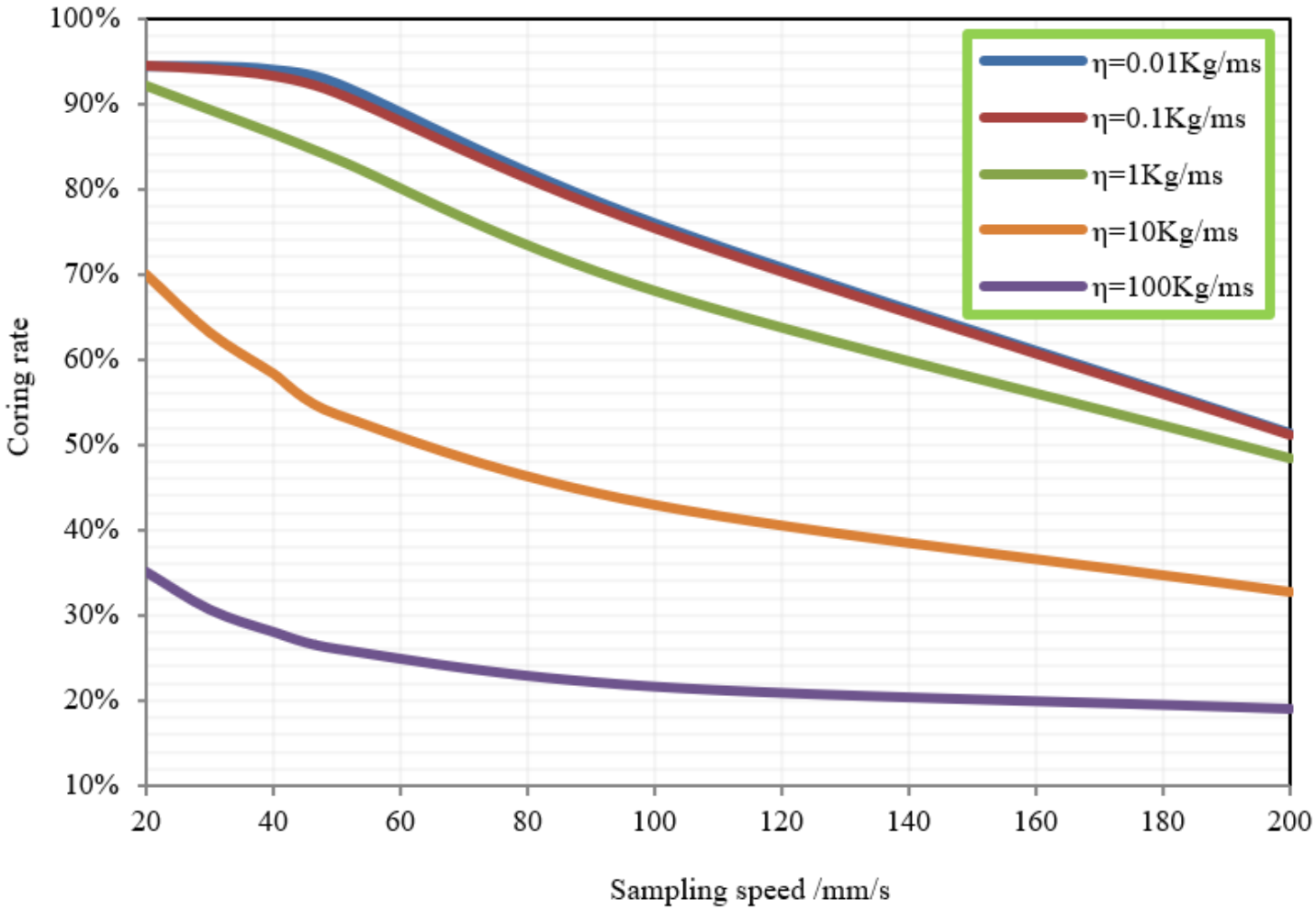

Figure 10

Relationship between the coring rate and sampling speed

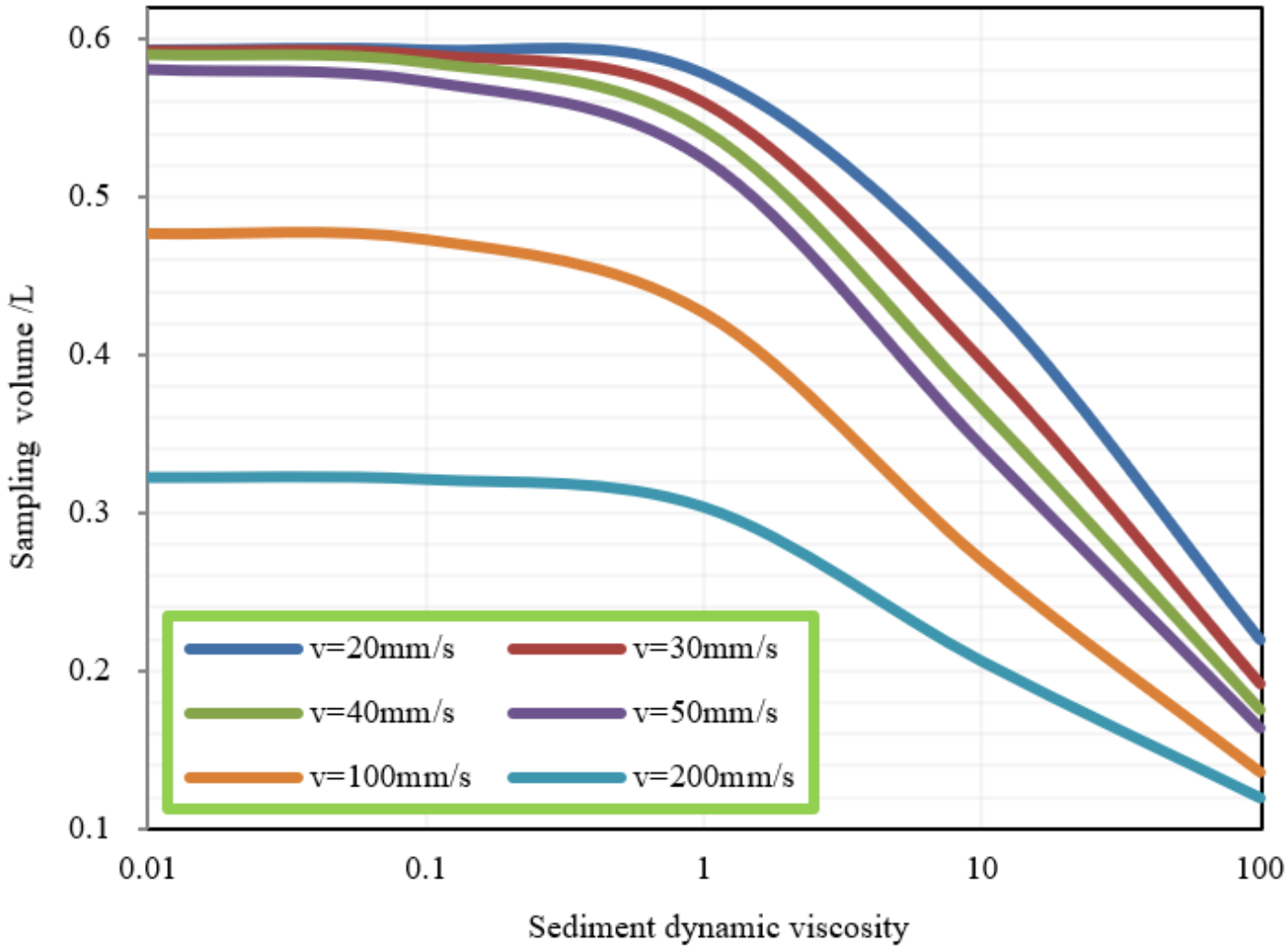

Figure 11

Relationship between the sampling volume and sediment viscosity

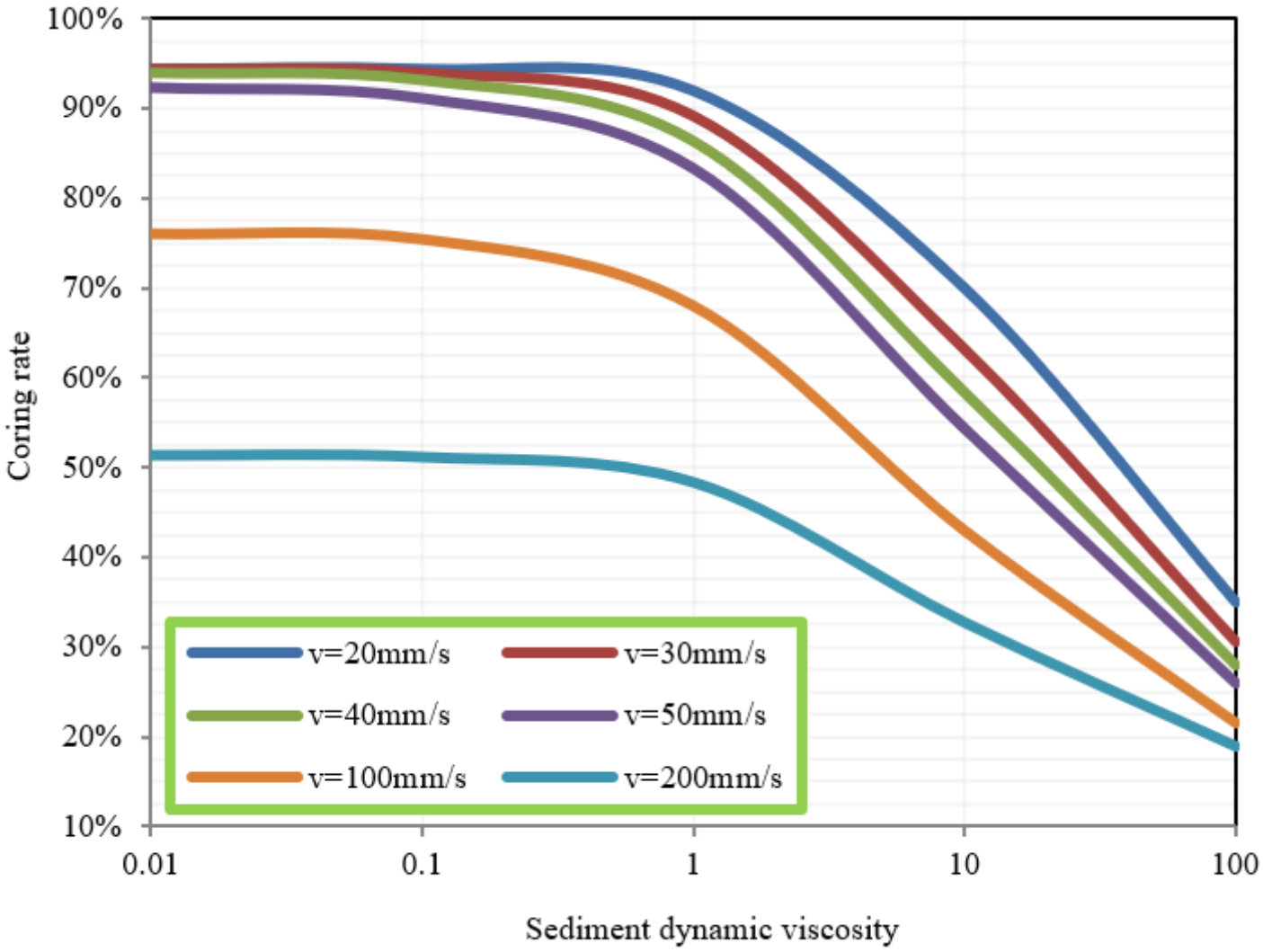

Figure 12

Relationship between the coring rate and sediment viscosity

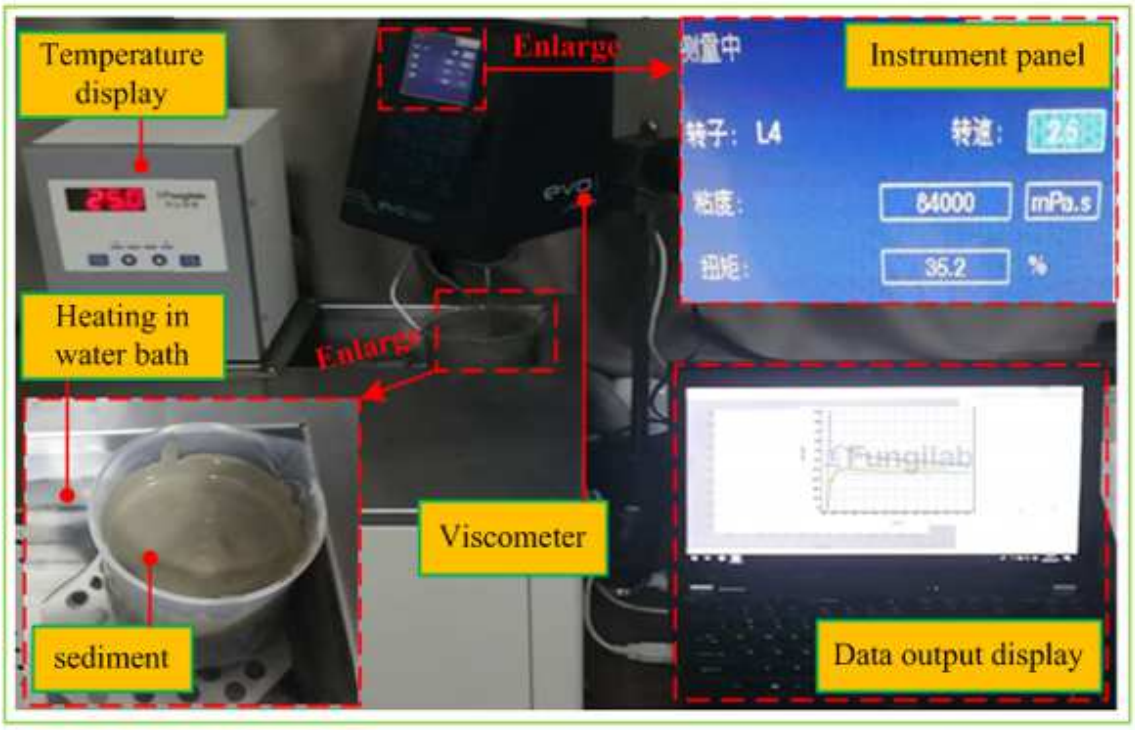

(a) Principle of measurement of experimental data

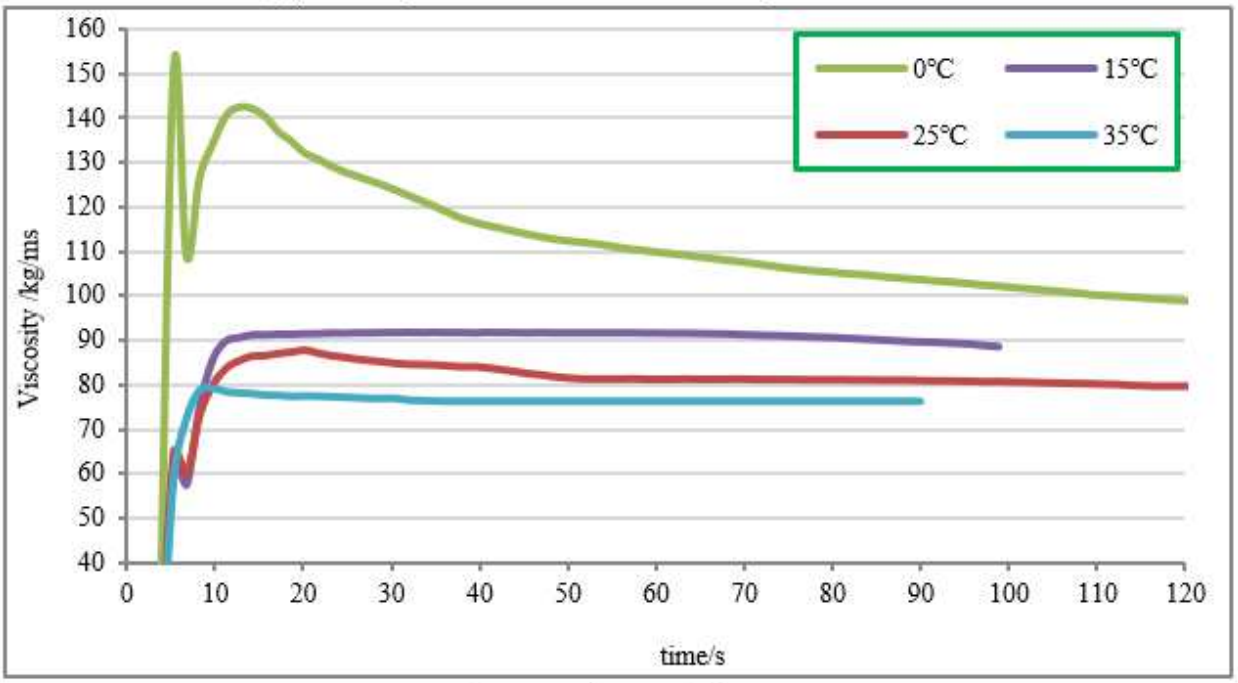

(b) Experimental data

Figure 13

Determination of dynamic viscosity of sediment

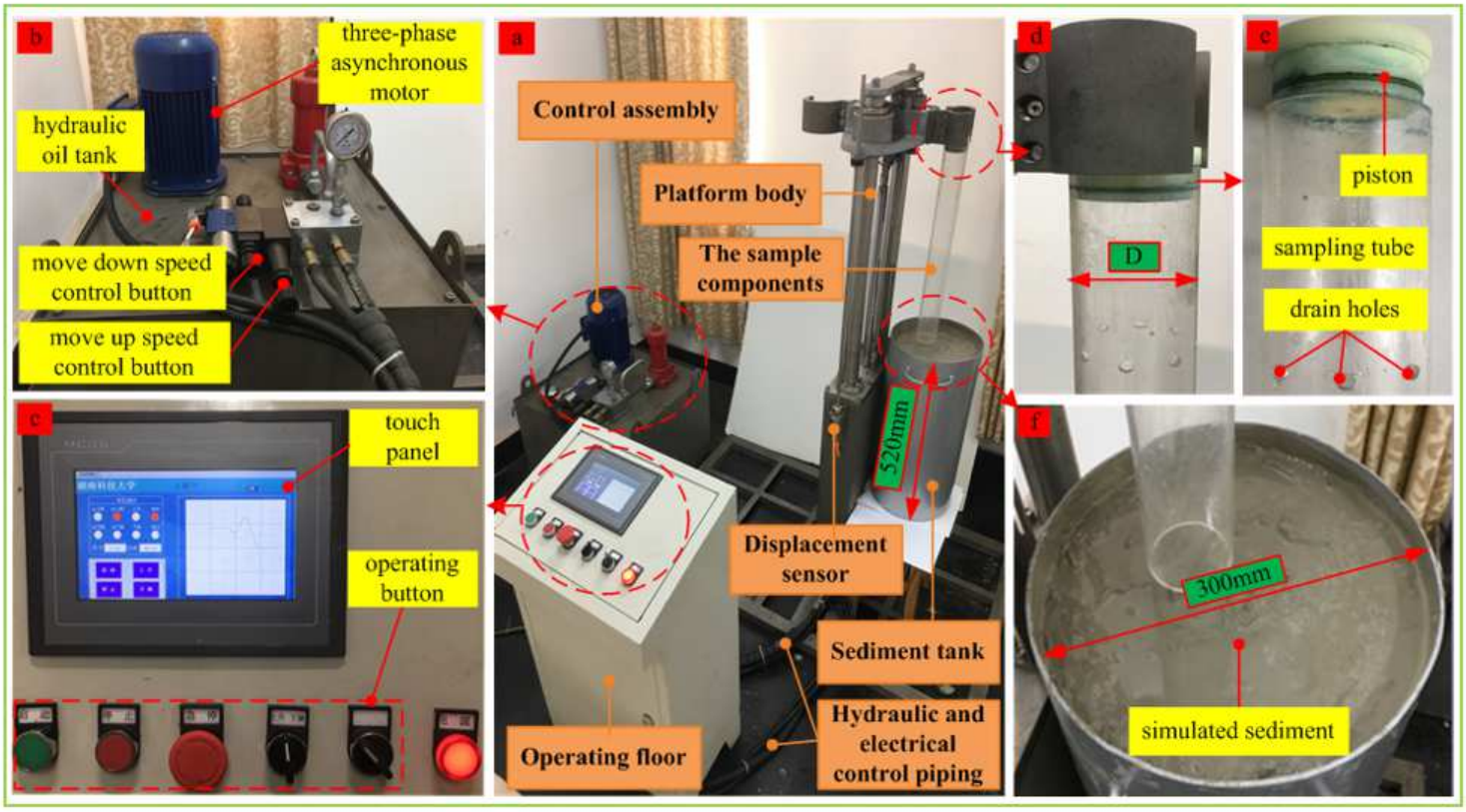

Figure 14

Design diagram of the experimental platform

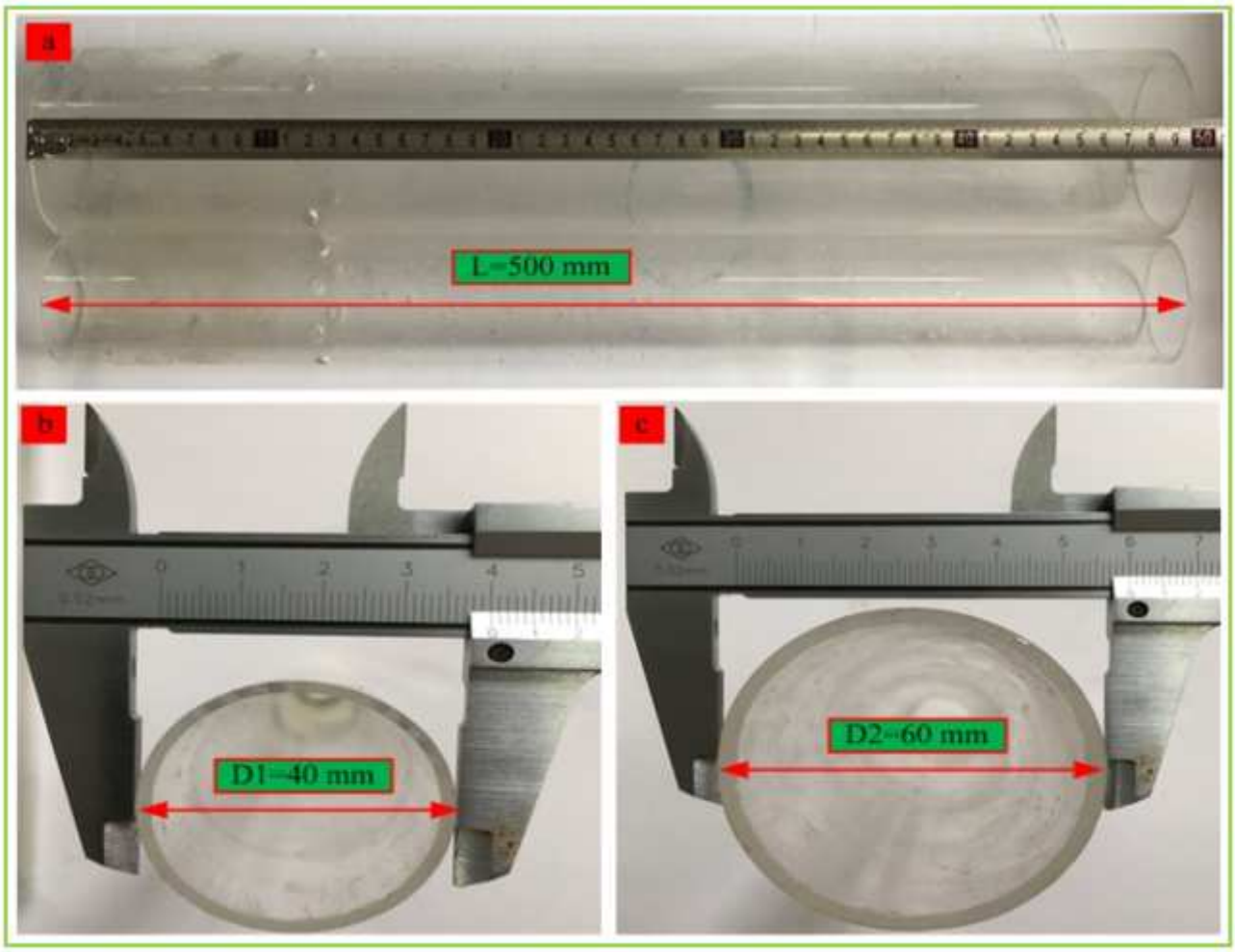

Figure 15

Size of the transparent circular tube

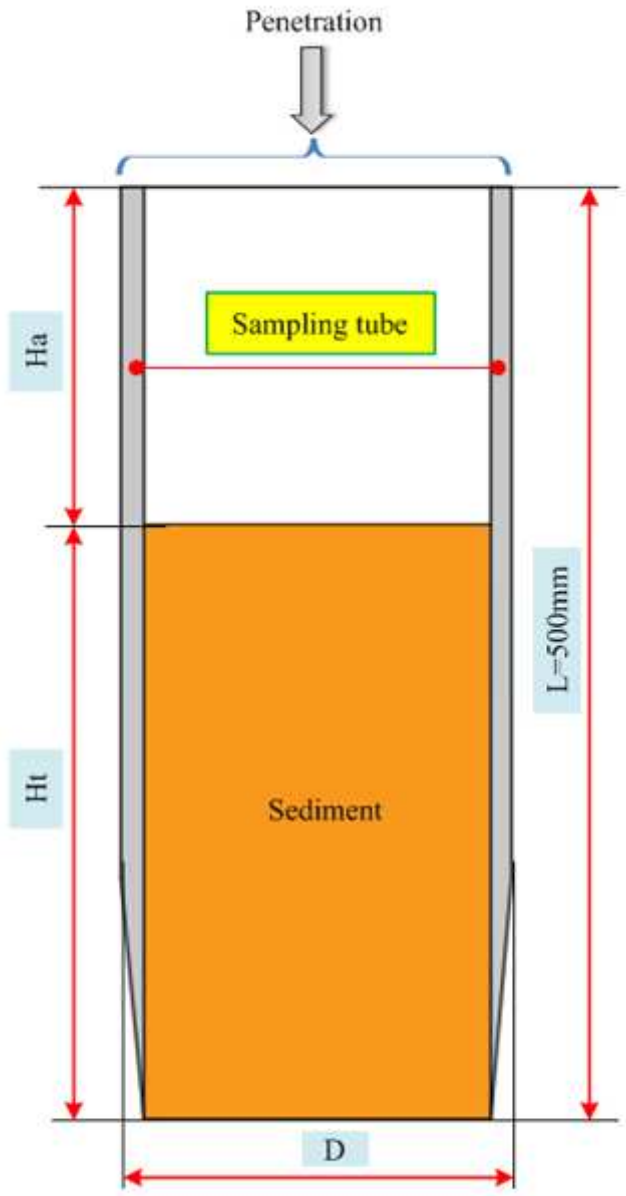

Figure 16

Measurement principle of experimental data

Figure 17

Field experiment and data measurement

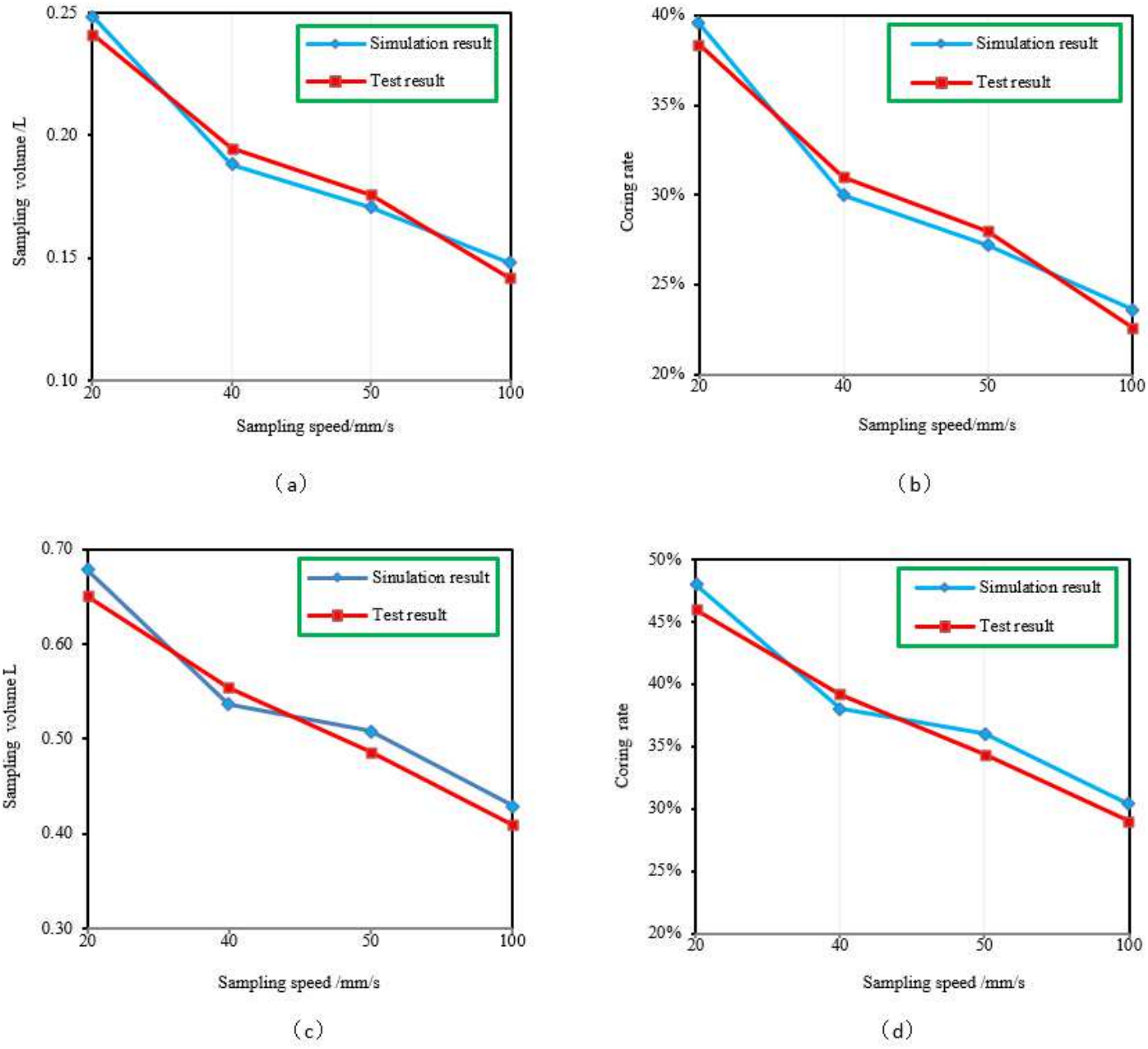

Figure 18

Comparison of simulation results and experimental results